CMS Physics Analysis Summary

Contact: cms-pag-conveners-susy@cern.ch 2016/08/04

Search for direct top squark pair production in the fully hadronic final state in proton-proton collisions at $\sqrt{s} = 13$ TeV corresponding to an integrated luminosity of 12.9 fb^{-1}

The CMS Collaboration

Abstract

A search for direct production of top squark pairs in events with jets and large transverse momentum imbalance is presented. The data were collected in proton-proton collisions at a center-of-mass energy of 13 TeV and correspond to an integrated luminosity of 12.9 fb^{-1}. Two analyses are performed, a "low Δm" analysis that targets scenarios with a very small difference in mass between the top squark and the neutralino, and a "high Δm" analysis that targets topologies typical for larger mass splittings. No significant excess of events above the expected background from standard model processes is observed. Exclusion limits are set in the context of simplified models of top squark pair production under various decay hypotheses, ranging up to 860 GeV in the case of the high Δm analysis and up to 450 GeV in the case of the low Δm analysis.

1 Introduction

This document presents a search for top squark pairs decaying to fully-hadronic final states, using 12.9 $\text{fb}^{-1}$of data collected in proton-proton collisions by the CMS detector in 2016 at a center-of-mass energy of 13 TeV. The search is based on methods described in Ref. [1] and represents an extension of the analysis described in that note to a significantly larger dataset, as well as to more challenging signal topologies.

Two analyses are performed, targeting different regions of signal parameter space. The first analysis, closely related to the "HPTT" analysis described in Ref. [1], probes signal scenarios in which the mass difference (Δm) between the top squark ($\widetilde{\text{t}}_1$) and the lightest neutralino ($\widetilde{\chi}_1^0$) is larger than the W boson mass. We refer to this as the "high Δm" analysis. The simplest decay modes in this case are $\widetilde{\text{t}}_1 \to \text{t}^{(*)}\widetilde{\chi}_1^0$ (the "T2tt" scenario) and $\widetilde{\text{t}}_1 \to \text{b}\widetilde{\chi}_1^{\pm} \to \text{bW}^{\pm(*)}\widetilde{\chi}_1^0$ (the "T2bW" scenario), with $\widetilde{\chi}_1^{\pm}$ representing the lightest chargino, and $\widetilde{\chi}_1^0$ the lightest neutralino, which is considered to be the stable LSP that escapes detection leading to large transverse momentum imbalance in the detector. Intermediate state particles marked by a parenthetical asterisk $(^*)$ may be virtual. We consider cases where both top squarks decay via one or the other of these decay modes, as illustrated in Fig. 1(a) and (b).

The second analysis, which we refer to as the "low Δm" analysis, is optimized for signal scenarios in which the mass difference between the $\widetilde{\text{t}}_1$ and $\widetilde{\chi}_1^0$ is less than the W boson mass. There are two main decay modes in such models: either through a flavor changing neutral current process ($\widetilde{\text{t}}_1 \to \text{c}\widetilde{\chi}_1^0$, where c is the charm quark), or through a four-body decay ($\widetilde{\text{t}}_1 \to \text{bf}\bar{\text{f}}\widetilde{\chi}_1^0$, Fig. 1(c)). The latter scenario will be referred to as the "T2fbd" scenario. The signature of such models is experimentally challenging since due to the small mass splitting between the $\widetilde{\text{t}}_1$ and the $\widetilde{\chi}_1^0$, the visible decay products are typically very soft, often escaping detection. However, such compressed scenarios are particularly interesting since their predicted dark matter relic density is consistent with cosmological observations [2]. We have therefore developed a dedicated search targeting this topology, exploiting the characteristics of such signals to attain improved sensitivity towards such scenarios compared to traditional SUSY searches.

In both analyses, we focus on the fully-hadronic final state, defined by an absence of isolated charged leptons, targeting signal events in which all W bosons produced in the top squark decay chains decay to quark pairs. This final state has the largest accessible branching ratio, thus compensating for the loss in signal acceptance due to the stringent requirements that must be placed on jets and transverse momentum imbalance in order to reduce the background originating from standard model (SM) processes. The main backgrounds that survive these requirements consist of events originating from $\text{t}\bar{\text{t}}$, W + jets, and single-top processes with at least one leptonic W boson decay, in which the lepton is not reconstructed or falls outside the kinematic acceptance, or from cases where a Z boson, produced in association with jets, decays to neutrinos. Significant missing transverse energy may be produced in such cases due to the presence of neutrinos or a "lost" lepton. A sub-dominant source of background originates from QCD multijet events in which significant mismeasurement of the momentum of one or more jets leads to large values of missing energy. Finally, we also consider rare standard model processes like the production of a Z boson in association with a pair of top quarks ($\text{t}\bar{\text{t}}\text{Z}$), which exhibits similar characteristics to the signal topologies targeted in the high Δm search and may therefore contribute noticeably to the total SM background in search regions defined by stringent selection criteria that strongly suppress the other background processes. Contributions from diboson processes are also included in the category of rare SM backgrounds.

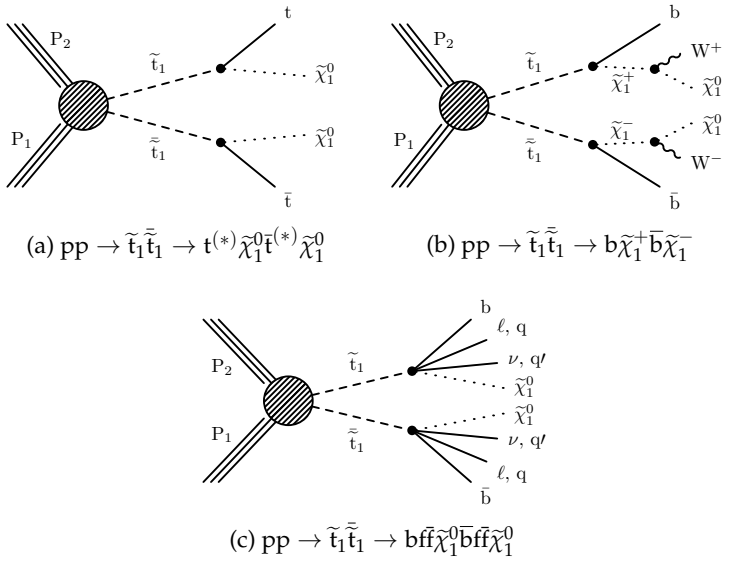

(a) $pp \to \tilde{t}_1\bar{\tilde{t}}_1 \to t^{(*)}\tilde{\chi}_1^0\bar{t}^{(*)}\tilde{\chi}_1^0$ (b) $pp \to \tilde{t}_1\bar{\tilde{t}}_1 \to b\tilde{\chi}_1^+\bar{b}\tilde{\chi}_1^-$

(c) $pp \to \tilde{t}_1\bar{\tilde{t}}_1 \to bf\bar{f}\tilde{\chi}_1^0\bar{b}f\bar{f}\tilde{\chi}_1^0$

Figure 1: Diagrams representing the pair production of top squarks and their subsequent decay modes that are studied in this document.

2 Event reconstruction and simulation

The event reconstruction is performed using the particle-flow (PF) algorithm [3, 4], combining information from the tracker, calorimeter, and muon systems in order to identify charged hadrons, neutral hadrons, photons, muons, and electrons in an event. The missing transverse momentum, $\vec{p}_{\mathrm{T}}^{\,\mathrm{miss}}$, is computed as the negative vector sum of the transverse momenta of all particle-flow (PF) candidates reconstructed in an event and its magnitude, $E_{\mathrm{T}}^{\mathrm{miss}}$, is an important discriminator between signal and background in both analyses. Events selected for the search are required to pass filters designed to remove detector- and beam-related noise and must have at least one reconstructed vertex. The reconstructed vertex with the largest $\sum p_{\mathrm{T}}^2$ of associated tracks is designated as the event primary vertex. Charged particles originating from the primary vertex, photons, and neutral hadrons are clustered into jets using the anti-k_{T} algorithm [5] with a distance parameter of 0.4. The jet energy is corrected to account for the contribution of additional pileup interactions in an event and to compensate for variations in the detector response. Selected jets are required to have their axes within the tracker volume, in the pseudo-rapidity range $|\eta| < 2.4$ and a minimum p_{T} of 20 GeV. Jets originating from b quarks are identified with the combined secondary vertex (CSV) algorithm [6, 7] using two different working points, referred to as loose and medium. The b tagging efficiency for jets originating from b quarks is about 80% (60%) for the loose (medium) working point, while the misidentification rates for jets from charm quarks, and from light quarks and gluons are about 45% (12%) and 10% (2%) respectively.

We reject events that contain isolated charged leptons in order to reduce SM backgrounds with intrinsic $E_{\mathrm{T}}^{\mathrm{miss}}$ such as leptonic $t\bar{t}$ and W+jets events. Electron candidates are first reconstructed by matching clusters of energy deposits in the electromagnetic calorimeter to reconstructed tracks. A number of selection criteria based on the shower shape, track-cluster matching, and consistency between the cluster energy and track momentum are then applied for the identification of electron candidates [8]. Muon candidates are reconstructed by requiring consistent hit patterns in the tracker and muon systems [9]. The relative isolation variable I_{rel} for electron and muon candidates is defined as the $\sum p_{\mathrm{T}}$ of PF candidates in a cone around the candidate's trajectory with a radius $R = \sqrt{(\Delta\eta)^2 + (\Delta\phi)^2}$, divided by the lepton p_{T}. The cone size depends

on the lepton p_T as follows:

$$\Delta R = \begin{cases} 0.2, & p_T \leq 50 \text{ GeV} \\ 10 \text{ GeV}/p_T, & 50 \text{ GeV} < p_T < 200 \text{ GeV} \\ 0.05, & p_T \geq 200 \text{ GeV} \end{cases} \quad (1)$$

The reduced cone radius for higher p_T candidates is motivated by the consideration that the decay products of more boosted heavy objects should have a smaller separation in $\eta - \phi$ space. The isolation sum is corrected for contributions originating from pileup interactions using an estimate of the pileup energy in the cone. Electron and muon candidates with $p_T > 5$ GeV and $|\eta| < 2.4$ are considered to be isolated if I_{rel} is less than 0.1 or 0.2 respectively.

Following the requirements on the presence or absence of isolated electrons and muons, a significant fraction of the remaining SM background originates from events with hadronically decaying tau leptons (τ_h). In order to reduce this background contribution, we veto events that have isolated charged hadron PF candidates with $p_T > 10$ GeV and $|\eta| < 2.4$ that are consistent with τ_h decays. The transverse mass of the candidate-$\vec{p}_T^{\,miss}$ system, M_T, is required to be less than 100 GeV so that the charged hadron and $\vec{p}_T^{\,miss}$ are consistent with having been produced by a W boson decay via a τ_h in order to avoid efficiency loss for signals with high jet multiplicity. The transverse mass for a particle q (in this case the τ_h candidate) is defined as:

$$M_T(q, E_T^{miss}) = \sqrt{2 q_T E_T^{miss} (1 - \cos \Delta\phi)} \ , \quad (2)$$

with q_T denoting the particle transverse momentum, and $\Delta\phi$ the azimuthal separation between the isolated candidate and $\vec{p}_T^{\,miss}$. The isolation requirement applied is based on a discriminant obtained from a multivariate boosted decision tree (BDT) trained to distinguish the characteristics of charged hadrons originating from τ_h decays from those of other particles [1]. The BDT input variables include the charged and total isolation sums within various ΔR cones around the candidate, distances in ΔR to the closest charged particle-flow candidate and the jet containing the τ_h candidate, and the b-tagging discriminant (CSV) value of that jet.

For signal models probed by the high Δm analysis that involve the production of highly boosted top quarks, it is possible to reconstruct the top quark decay products within a single large-radius jet. In less boosted scenarios, or in models that do not involve on-shell top quarks, the hadronic decay products of the W bosons may be reconstructed in a similar manner. The reconstruction of hadronically decaying top quark or W boson candidates is an important component of the high Δm analysis, used to distinguish signal events while strongly suppressing background processes. The decay products of boosted top quarks with $p_T > 400$ GeV, or of W bosons with $p_T > 200$ GeV, are expected to be contained within a radius of 0.8 in $\eta - \phi$ space. In this analysis, we use jets clustered with the anti-k_T algorithm using a distance parameter (R) of 0.8, and then re-clustered using the Cambridge-Aachen algorithm, as candidates for the reconstruction of the hadronic decay products of boosted top quarks and W bosons merged within a single jet. Top quark and W boson candidates are identified with the help of requirements on the jet mass reconstructed by the soft drop algorithm [10], and on the N-subjettiness (τ_N) variables [11]. A candidate large-R jet is identified as being top-tagged if its soft drop mass is between 110 GeV and 210 GeV, i.e. consistent with the top quark mass, and if the observable $\tau_{32} \equiv \tau_3/\tau_2$ is less than 0.69, or as being W-tagged if its soft drop mass is between 60 GeV and 110 GeV (consistent with the W boson mass) and the observable $\tau_{21} \equiv \tau_2/\tau_1$ is less than 0.6. Large-R jets must have a minimum p_T of 400 (200) GeV in order to be selected as candidates

for top (W) tagging. The clustering of these large-R jets and the selection of top- or W-tagged candidates is independent of the reconstruction and selection of jets with $R = 0.4$.

Monte Carlo (MC) simulations of event samples are used to study the properties of the SM background processes and signal models. The MADGRAPH5 generator [12] is used to simulate events originating from $\mathrm{t\bar{t}}$, W+jets, Z +jets, γ+jets and QCD multijet processes and from signal production based on leading order (LO) NNPDF3.0 [13] parton distribution functions (PDFs). Single-top events produced in the tW channel and WW events are generated with POWHEG v1.0 [14–17], while the WZ and ZZ processes and rare SM processes such as $\mathrm{t\bar{t}Z}$ and $\mathrm{t\bar{t}W}$ are generated using the MADGRAPH5_AMC@NLO program [18]. Next-to-leading order (NLO) NNPDF3.0 PDFs are used in both cases. The parton showering and hadronization is simulated with PYTHIA8.1 [19]. A GEANT4-based model [20] is used to simulate the response of the CMS detector in the case of the SM background. The CMS fast simulation package [21] is used in the case of signal samples and is verified to provide results that are consistent with those obtained from the full GEANT4-based simulation. Event reconstruction is performed in the same manner as for collision data. A nominal distribution of pileup interactions is used when producing the simulated samples. The samples are then reweighted in order to match the pileup profile observed in the collected data. The signal production cross sections are calculated using NLO plus next-to-leading logarithm (NLL) calculations [22]. The most precise available cross section calculations are used to normalize the SM simulated samples, corresponding to next-to-next-to-leading order (NNLO) accuracy in most cases.

In cases where the simulation does not adequately describe the data, correction factors are applied to account for the observed discrepancies. Differences in the efficiencies for selecting isolated leptons between simulation and data are measured in $\mathrm{Z} \to \ell\ell$ events in the case of electrons and muons and in a $\mathrm{t\bar{t}}$-enriched sample for hadronic taus. The observed deviations are accounted for in the form of corrections to the simulation, and the corresponding uncertainties are propagated to the predicted SM yields in the search regions. Uncertainties related to the calibration of the jet energy in simulation to match the data are considered. Correction factors and uncertainties based on measurements of b tagging performance in data and simulation [23] are also applied. They are parameterized by jet kinematics and flavor. An additional uncertainty related to the pileup reweighting procedure is taken into account for the simulation.

The top and W tagging efficiency and mis-identification rate are measured in data and compared to the expectation from simulation. The tagging efficiency is estimated in a sample dominated by semi-leptonic $\mathrm{t\bar{t}}$ events that are selected using a single muon trigger. The muon in the event is required to have $p_{\mathrm{T}} > 50$ GeV and $|\eta| < 2.1$. To suppress other backgrounds, at least one b-tagged jet in the same hemisphere as the muon is required. The top and W candidates are required to lie in the hemisphere opposite to the muon. The contamination from QCD multijet events is reduced to small levels by requiring $E_{\mathrm{T}}^{\mathrm{miss}} > 100$ GeV and candidate jet soft drop mass $M_{\text{soft drop}} > 30$ GeV. The latter criterion is over 99% efficient, as measured in simulation, for the $p_{\mathrm{T}} > 200$ GeV candidates originating from top and W decays. Therefore this loose selection effectively reduces background events without significantly biasing the efficiency measurement. The observed efficiency is similar to the efficiency estimated in simulation for the W tagging and $\sim 10\%$ lower for the top tagging. The measured data-to-simulation efficiency ratios are propagated to the signal simulation, parameterized by the candidate p_{T}, and an uncertainty in the correction corresponding to one-half of its size is assigned.

Signal samples produced by fast simulation are corrected in a similar way for differences in top and W tagging efficiencies with respect to full simulation samples using correction factors derived in a $\mathrm{t\bar{t}}$-enriched sample requiring $E_{\mathrm{T}}^{\mathrm{miss}} > 200$ GeV and two or more jets. The efficiencies

for both top and W tagging in fast simulation are up to $\sim 5\%$ higher than in full simulation in certain ranges of candidate p_{T}. The efficiencies for selecting candidates in these p_{T} ranges are corrected and assigned an uncertainty corresponding to one-half the size of the correction. For p_{T} ranges in which the efficiencies are measured to be consistent within statistical uncertainties, a systematic uncertainty of 3% is assigned.

3 Analysis strategy

3.1 The high Δm analysis

The data used in this analysis are recorded by requiring the presence of $E_{\mathrm{T}}^{\mathrm{miss}} > 100$ GeV and $H\!\!\!/_{\mathrm{T}} > 100$ GeV in the high-level trigger, where the observable $H\!\!\!/_{\mathrm{T}}$ is the magnitude of $\vec{H}_{\mathrm{T}}^{\mathrm{miss}}$, the negative vectorial sum of the p_{T} of jets with $p_{\mathrm{T}} > 20$ GeV in an event. The trigger is found to be $>$ 98% efficient for events selected offline with $E_{\mathrm{T}}^{\mathrm{miss}} > 250$ GeV.

A loose pre-selection, which we will refer to as the *high Δm baseline selection*, that places additional criteria on jets and $E_{\mathrm{T}}^{\mathrm{miss}}$ is then used to eliminate a large fraction of background events. This baseline selection is defined by the absence of isolated electron, muon, and hadronic tau candidates, $E_{\mathrm{T}}^{\mathrm{miss}} > 250$ GeV, at least five jets, at least two of which satisfy the loose CSV working point with at least one satisfying the medium working point, and $\Delta\phi_{1234} > 0.5$, where

$$\Delta\phi_{1234} \equiv \mathrm{Min}[|\Delta\phi(E_{\mathrm{T}}^{\mathrm{miss}}, \mathrm{j}_1)|, |\Delta\phi(E_{\mathrm{T}}^{\mathrm{miss}}, \mathrm{j}_2)|, |\Delta\phi(E_{\mathrm{T}}^{\mathrm{miss}}, \mathrm{j}_3)|, |\Delta\phi(E_{\mathrm{T}}^{\mathrm{miss}}, \mathrm{j}_4)|] \ , \tag{3}$$

and $\mathrm{j}_1, \mathrm{j}_2, \mathrm{j}_3, \mathrm{j}_4$ are the four leading jets in p_{T}. The requirements on the azimuthal angles, $\Delta\phi$, between the four leading jets and the azimuthal direction of $E_{\mathrm{T}}^{\mathrm{miss}}$ reduce the contribution of the QCD multijet background in the final search regions to a negligible level.

Imposing a minimum requirement of 175 GeV on the m_{T} between the two most b-like jets and the $E_{\mathrm{T}}^{\mathrm{miss}}$, namely:

$$\mathrm{Min}[m_{\mathrm{T}}(\mathrm{b}_1, E_{\mathrm{T}}^{\mathrm{miss}}), m_{\mathrm{T}}(\mathrm{b}_2, E_{\mathrm{T}}^{\mathrm{miss}})] \equiv M_{\mathrm{T}}(\mathrm{b}_{1,2}, E_{\mathrm{T}}^{\mathrm{miss}}) \ , \tag{4}$$

where $\mathrm{b}_1, \mathrm{b}_2$ are the two selected b-tagged jets with the highest values of the CSV discriminator, reduces a significant portion of the $\mathrm{t\bar{t}}$ background as seen in Fig. 2. The majority of the $\mathrm{t\bar{t}}$ background stems from $\mathrm{t\bar{t}}$ events where one of the W bosons undergoes a leptonic decay and the lepton is missed, leading to $E_{\mathrm{T}}^{\mathrm{miss}}$. Hence, the transverse mass of $E_{\mathrm{T}}^{\mathrm{miss}}$ and the b-quark from the same top decay as the missed lepton has an endpoint at the mass of the top quark. However, this requirement may be inefficient for signal models with moderate-to-small differences in mass between the $\tilde{\mathrm{t}}_1$ and the $\tilde{\chi}_1^0$. In order to benefit from the separation power provided by this variable, two search regions are defined, one with $M_{\mathrm{T}}(\mathrm{b}_{1,2}, E_{\mathrm{T}}^{\mathrm{miss}}) \geq 175$ GeV taking advantage of the reduction of the $\mathrm{t\bar{t}}$ background in the high $M_{\mathrm{T}}(\mathrm{b}_{1,2}, E_{\mathrm{T}}^{\mathrm{miss}})$ region, and one with $M_{\mathrm{T}}(\mathrm{b}_{1,2}, E_{\mathrm{T}}^{\mathrm{miss}}) < 175$ GeV, ensuring that the statistical power of the low $M_{\mathrm{T}}(\mathrm{b}_{1,2}, E_{\mathrm{T}}^{\mathrm{miss}})$ region is not lost.

Signal events with hadronically decaying top quarks should have at least six jets in the final state. Additional jets may also be produced through initial state radiation (ISR). The jet multiplicity (N_{j}) is lower for the semi-leptonic $\mathrm{t\bar{t}}$ background, as well as for the other backgrounds remaining after the baseline selection. A requirement of higher reconstructed jet multiplicity therefore improves the discrimination of signal events from the SM background. We define two regions in jet multiplicity for this analysis, a high N_{j} region (≥ 7 jets) that benefits from this improved discrimination, and a medium N_{j} region ($5-6$ jets) to retain signal events with fewer reconstructed jets. The high N_{j} region in combination with the low threshold on the p_{T}

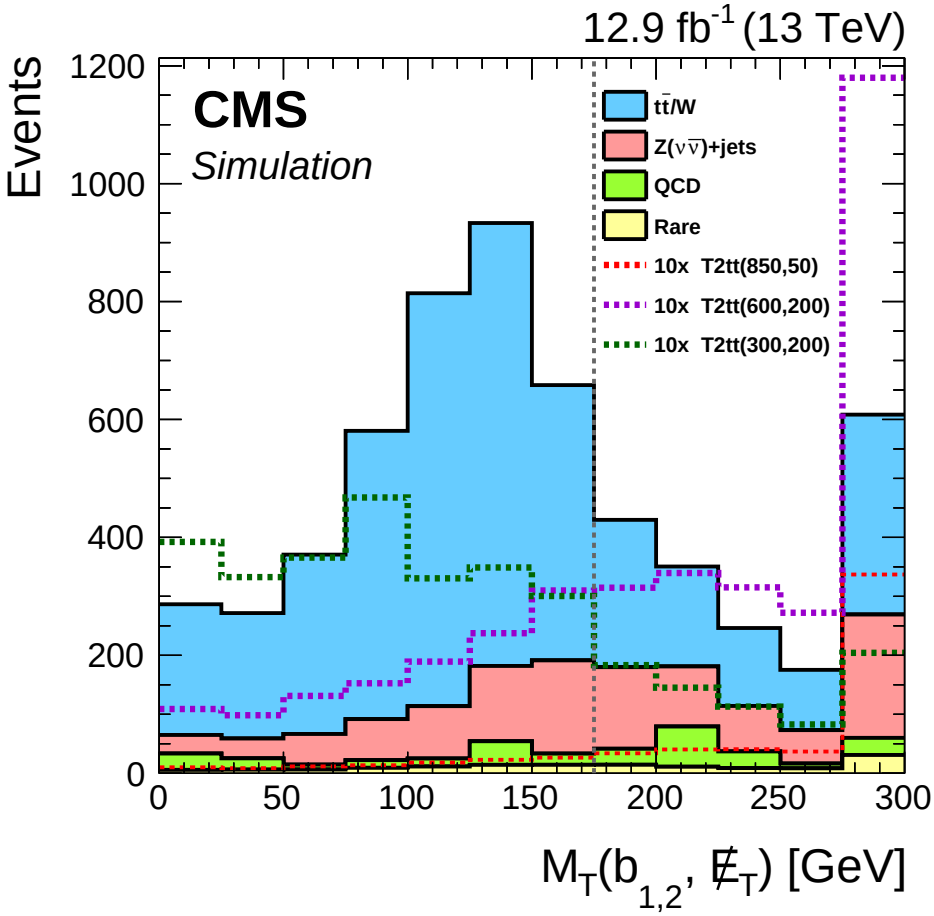

Figure 2: $M_{\mathrm{T}}(\mathrm{b}_{1,2}, E_{\mathrm{T}}^{\mathrm{miss}})$ distribution after the high Δm baseline selection for simulated events, normalized to an integrated luminosity of 12.9 fb^{-1}. The expected signal yields are scaled by a factor of ten to facilitate a comparison with the expected SM backgrounds. Events surviving the high Δm baseline selection are separated into categories defined by $M_{\mathrm{T}}(\mathrm{b}_{1,2}, E_{\mathrm{T}}^{\mathrm{miss}}) < 175$ GeV and $M_{\mathrm{T}}(\mathrm{b}_{1,2}, E_{\mathrm{T}}^{\mathrm{miss}}) \geq 175$ GeV.

of selected jets is designed to provide additional handles to target signal models with softer decay products in the final state.

In the high $M_{\mathrm{T}}(\mathrm{b}_{1,2}, E_{\mathrm{T}}^{\mathrm{miss}})$ region, requiring at least one top-tagged or W-tagged jet can be used to ensure high signal purity at the cost of a depletion of the potential signal yield. The top and W tag selections are orthogonal and can therefore be used in conjunction with each other to improve signal sensitivity. A top tagging requirement ensures a very pure selection of signal events with boosted top quarks but is only efficient for signal models with large $\Delta m(\tilde{\mathrm{t}}_1, \tilde{\chi}_1^0)$ for which heavily boosted top quarks are likely to be produced. Requiring one or more W-tagged candidates therefore helps to recover signal efficiency in cases that the top quarks are not sufficiently boosted to have their decay products merged into a single jet. Additionally, in signal scenarios with two on-shell top quarks, depending on their $m_{\tilde{\mathrm{t}}_1}, m_{\tilde{\chi}_1^0}$ configurations, one top quark can have very high p_{T} while the other is only moderately boosted. Requiring the presence of both a top-tagged and a W-tagged jet in such scenarios provides excellent signal purity while still maintaining reasonable signal efficiency. Consequently, four exclusive event categories based on the number of reconstructed top and W tags (N_{t} and N_{W}) are defined in the high $M_{\mathrm{T}}(\mathrm{b}_{1,2}, E_{\mathrm{T}}^{\mathrm{miss}})$ region: $N_{\mathrm{t}} \geq 1, N_{\mathrm{W}} \geq 1$; $N_{\mathrm{t}} \geq 1, N_{\mathrm{W}} = 0$; $N_{\mathrm{t}} = 0, N_{\mathrm{W}} \geq 1$; and $N_{\mathrm{t}} = 0, N_{\mathrm{W}} = 0$ in order to retain the statistical power of signal events that fail both the top and W tagging requirements. The subdivision in N_{j} described above is only performed in the $N_{\mathrm{t}} = 0, N_{\mathrm{W}} = 0$ region, since it would not benefit the much smaller samples of events that survive the top or W tagging selections.

Events in all of the above categories are further separated by the number of reconstructed b-jets into $N_{\mathrm{b}} = 1$ and $N_{\mathrm{b}} \geq 2$ categories as this provides even greater discrimination of signal from background. Finally, $E_{\mathrm{T}}^{\mathrm{miss}}$ is used to characterize and distinguish a potential signal from SM background. The definitions of the final 60 disjoint search regions are listed in Table 1.

Table 1: Summary of the 60 disjoint search regions used in the high Δm analysis.

Category	$M_{\mathrm{T}}(\mathrm{b}_{1,2}, E_{\mathrm{T}}^{\mathrm{miss}}) < 175$ GeV				$M_{\mathrm{T}}(\mathrm{b}_{1,2}, E_{\mathrm{T}}^{\mathrm{miss}}) \geq 175$ GeV									
$N_{\mathrm{t}}/N_{\mathrm{W}}$	–				$N_{\mathrm{t}} = 0, N_{\mathrm{W}} = 0$				$N_{\mathrm{t}} \geq 1, N_{\mathrm{W}} = 0$		$N_{\mathrm{t}} = 0, N_{\mathrm{W}} \geq 1$		$N_{\mathrm{t}} \geq 1, N_{\mathrm{W}} \geq 1$	
N_{j}	5−6		≥ 7		5−6		≥ 7		≥ 5		≥ 5		≥ 5	
N_{b}	1	≥ 2	1	≥ 2	1	≥ 2	1	≥ 2	1	≥ 2	1	≥ 2	1	≥ 2
$E_{\mathrm{T}}^{\mathrm{miss}}$ [GeV]	250−300 300−400 400−500 ≥ 500	250−300 300−400 400−500 ≥ 500	250−300 300−400 400−500 ≥ 500	250−300 300−400 400−500 ≥ 500	250−350 350−450 450−550 ≥ 550	250−350 350−450 450−550 ≥ 550	250−350 350−450 450−550 ≥ 550	250−350 350−450 450−550 ≥ 550	250−350 350−450 450−550 550−650 ≥ 650	250−350 350−450 450−550 550−650 ≥ 650	250−350 350−450 450−550 550−650 ≥ 650	250−350 350−450 450−550 550−650 ≥ 650	250−350 350−450 450−550 ≥ 500	250−300 300−400 400−500 ≥ 500

3.2 The low Δm analysis

This analysis is based on events collected with the same trigger that is used for the high Δm analysis. The event pre-selection (the *low Δm baseline selection*) first requires the absence of isolated electrons, muons, and hadronic tau candidates, and $E_{\mathrm{T}}^{\mathrm{miss}} > 250$ GeV. Next, we try to access signal topologies in which the $\tilde{\mathrm{t}}_1\bar{\tilde{\mathrm{t}}}_1$ pair recoils against initial-state radiation (ISR), giving sufficient momentum to the generally soft decay products that arise in models with small mass splittings between the $\tilde{\mathrm{t}}_1$ and $\tilde{\chi}_1^0$ such that the events can enter our search sample. We therefore require $N_{\mathrm{ISR}} \geq 1$, ($p_{\mathrm{T}}(ISR) > 250$ GeV, $|\eta| < 2.4$, $|\Delta\phi(j_{\mathrm{ISR}}, E_{\mathrm{T}}^{\mathrm{miss}})| > 2$), where N_{ISR} is the number of selected jets failing loose CSV working point. In order to suppress the QCD multijet background that can once again enter the search sample through the significant mismeasurement of one or more jets in the event, we require $|\Delta\phi(\mathrm{j}_1, \not{E}_{\mathrm{T}})| > 0.5$, $|\Delta\phi(\mathrm{j}_{2,3}, \not{E}_{\mathrm{T}})| > 0.15$, where $\mathrm{j}_1, \mathrm{j}_2, \mathrm{j}_3$ are the three leading jets in p_{T}, and missing transverse energy significance $E_{\mathrm{T}}^{\mathrm{miss}}/\sqrt{H_{\mathrm{T}}} \equiv S_{\not{E}_{\mathrm{T}}} > 10$, where H_{T} is calculated as the scalar sum of the p_{T} of all jets in the event.

Events passing the baseline selection are distributed into three categories based on N_b, the number of b-jets tagged with the medium working point, and N_b^L, the number of b-jets tagged with the loose working point. The zero-b tag category, defined by the requirement $N_b = 0$, is used to target very compressed mass configurations. The one- and two- b tag categories, separated from the zero-b tag category by requiring $N_b \geq 1$, are then defined by requirements on the number of loose b-tagged jets ($N_b^L = 1$ and $N_b^L \geq 2$ respectively). All three categories are subdivided into two "ISR regions" based on p_T(ISR): p_T(ISR) $\in [250, 500)$ GeV and p_T(ISR) $>$ 500 GeV. Only the high ISR region is used in the search in the case of the zero-b tag category since the lower ISR region does not provide much signal sensitivity in this case.

The events in the zero-b tag, high ISR category are further divided into two regions based on N_j. A high N_j region ($\geq$ 6 jets) benefits from improved discrimination in four-body decay scenarios, and the low N_j region ($2-5$ jets) retains signal events with fewer reconstructed jets for all signal scenarios. The high N_j region in conjunction with the low threshold on the p_T of selected jets helps in the discrimination of signal models with soft decay products in the final state, but nevertheless featuring additional jets due to initial-state radiation, from background.

In the $N_b \geq 1$ categories the kinematic properties related to the reconstructed b jet(s) help to significantly suppress SM backgrounds. Events are selected if they satisfy the requirement $M_T(b_{1,2}, E_T^{miss}) < 100$ GeV. In events where only one of the reconstructed jets satisfies the loose b-tag working point, this jet alone is used for the calculation of $M_T(b_{1,2}, E_T^{miss})$. In four body decay signal models, the $\widetilde{\chi}_1^0$ is much heavier than the other decay products of the $\widetilde{t}_1$ and hence carries most of the $\widetilde{t}_1$ momentum. As a consequence the b quarks and other fermions are very soft. We utilize this fact to further distinguish signal from background, by categorizing the events based on the transverse momentum of the b-quarks, $p_T(b)$. Events in the one-b tag category are subdivided into regions defined by $p_T(b) \in [20, 40), [40, 70)$ GeV, while those in the two-b tag category are separated into regions defined by $p_T(b_{12}) \equiv (p_T(b_1) + p_T(b_2)) \in [40, 100), [100, 160)$ GeV. As seen in Fig. 3 which shows the expected $p_T(b_{12})$ distribution for events in the two-b tag category, we benefit from this categorization since the p_T spectrum of the b jets originating from signal events is considerably softer than that of the background. Finally, E_T^{miss} is used as the final search variable to discriminate a potential signal from the SM background.

The definitions of the 40 disjoint search regions are summarized in Table 2. These search regions contain some overlap of events with the search regions defined for the high Δm analysis. Each set of search regions is therefore used independently in the statistical interpretation of the results of the search in the context of the high Δm and low Δm signal scenarios respectively.

Table 2: Summary of the 40 search regions used in the low Δm analysis.

Category	$N_b = 0$		$N_b \geq 1, N_b^L = 1$				$N_b \geq 1, N_b^L \geq 2$			
p_T(ISR)	>500		250−500		>500		250−500		>500	
N_j	$2-5$	≥ 6	≥ 2		≥ 2		≥ 3		≥ 3	
$p_T(b)$ or $p_T(b_{12})$	−		$20-40$	$40-70$	$20-40$	$40-70$	$40-100$	$100-160$	$40-100$	$100-160$
E_T^{miss} [GeV]	450−550	450−550	300−400	300−400	450−550	450−550	300−400	300−400	450−550	450−550
	550−650	550−650	400−500	400−500	550−650	550−650	400−500	400−500	550−650	550−650
	650−750	650−750	500−600	500−600	650−750	650−750	500−600	500−600	650−750	650−750
	>750	>750	>600	>600	>750	>750	>600	>600	>750	>750

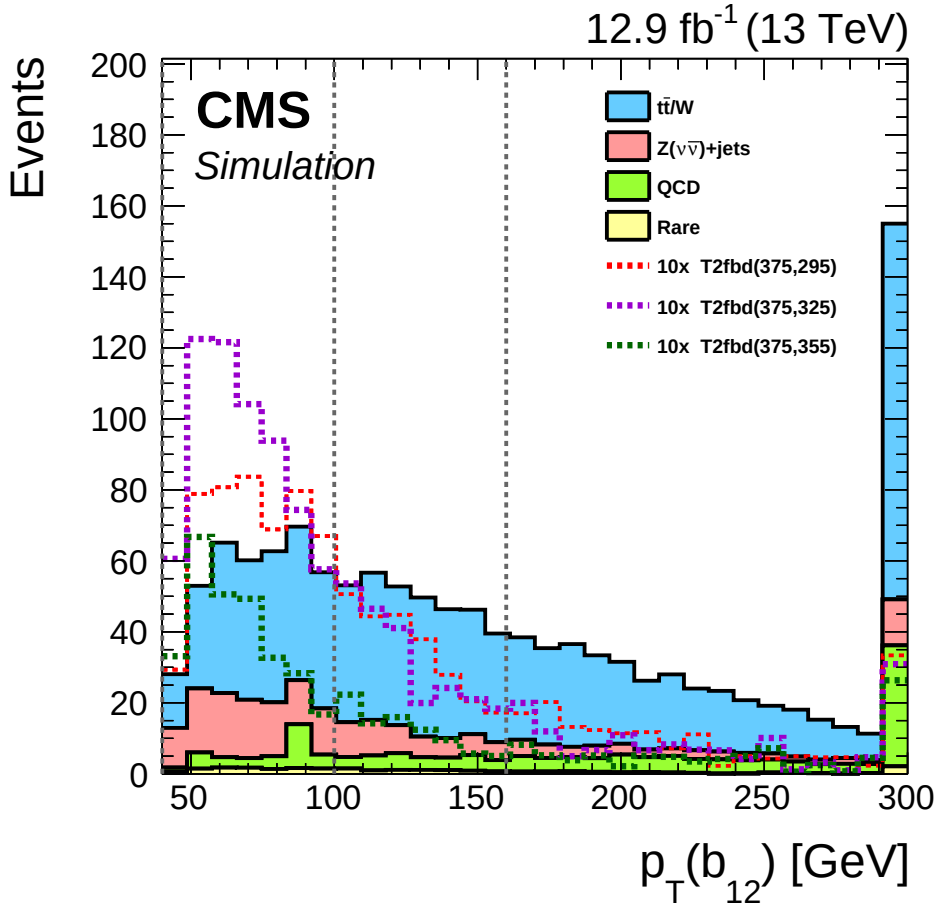

Figure 3: $p_{\mathrm{T}}(\mathrm{b}_{12})$ distribution after the low Δm baseline selection in the two b tag category for simulated events, normalized to an integrated luminosity of 12.9 fb^{-1}. The expected signal yields are scaled by a factor of ten to facilitate a comparison with the expected SM backgrounds. Events entering the two b tag category of the low Δm analysis are subdivided into categories defined by $p_{\mathrm{T}}(\mathrm{b}_{12}) \in [40, 100), [100, 160)$ GeV.

4 Background estimation

The estimation of the main backgrounds in the search regions is obtained using dedicated data control samples, with the help of simulation samples that are used to translate the observations in the control samples into estimates of the background contributions in the search regions.

4.1 Estimation of the lost lepton background

The contribution from the $\mathrm{t\bar{t}}$ and W+jets processes arises from leptonic decays of the W boson where the charged lepton is outside the kinematic acceptance of CMS or evades identification by the dedicated lepton vetoes. Large $E_{\mathrm{T}}^{\mathrm{miss}}$ can be generated by the associated neutrino and the lepton that is not reconstructed, allowing such events to enter the search regions. This background is collectively referred to as the "Lost Lepton" (LL) background. Contributions arising from $\mathrm{t\bar{t}W}$ and single top quark processes also enter into this category, but with much smaller importance.

We use a single-lepton control sample, consisting of events that have at least one lepton satisfying the lepton-veto criteria, to estimate this background. In order to suppress potential signal contamination, we require $M_{\mathrm{T}}(\ell, E_{\mathrm{T}}^{\mathrm{miss}}) < 100$ GeV. If there is more than one selected lepton, we randomly select which lepton is chosen to determine the $M_{\mathrm{T}}(\ell, E_{\mathrm{T}}^{\mathrm{miss}})$. The selection applied to the single-lepton control sample follows the same selection on the search variables as in the zero-lepton selection. The lost lepton estimation in each search region is based upon the event count observed in data for the corresponding control region in the single-lepton sample. The count is extrapolated to the search region to obtain a prediction by means of a transfer factor obtained from simulation samples as follows:

$$N_{\mathrm{pred}}^{\mathrm{LL}} = TF_{\mathrm{LL}} \cdot N_{\mathrm{data}}(1\ell), \tag{5}$$

where $N_{\mathrm{data}}(1\ell)$ corresponds to the event counts observed in the relevant control region. The factor, TF_{LL}, used to translate the results to a prediction is defined as:

$$TF_{\mathrm{LL}} = \frac{N_{\mathrm{MC}}(0\ell)}{N_{\mathrm{MC}}(1\ell)} \ , \tag{6}$$

where $N_{\mathrm{MC}}(0\ell)$ and $N_{\mathrm{MC}}(1\ell)$ are the expected LL yields in simulation in the zero- and single-lepton samples, respectively, taking into account contributions from $\mathrm{t\bar{t}}$ and W+jets events and the smaller contributions from single top quark and $\mathrm{t\bar{t}W}$ processes. This method is used to estimate the lost lepton background in the high Δm search regions.

The method described above can be limited by statistical uncertainties in search regions defined with more stringent selection criteria. This is especially important for the low Δm search regions, which generally extend further in $E_{\mathrm{T}}^{\mathrm{miss}}$ and ISR boost in order to attain sufficient signal sensitivity. For these signal regions, we therefore use a similar method that yields smaller statistical uncertainties. This method relies on the fact that the dominant sources of potential differences between data and simulation are mainly related to the description of the transverse momentum of the W bosons ($p_{\mathrm{T}}(\mathrm{W})$). The single-lepton control sample is used to extract such corrections. The W boson candidate p_{T} in the control sample is obtained as the vector sum of $\vec{p}_{\mathrm{T}}^{\,lep}$ and $E_{\mathrm{T}}^{\mathrm{miss}}$. The control sample is recorded with a suite of triggers requiring the presence of a single electron or muon, and consists of events with exactly one electron or muon satisfying slightly more stringent lepton selection requirements than those imposed for the lepton vetoes, in order to ensure a higher purity selection. To suppress contamination from QCD multijet processes, events in the control sample are required to have $E_{\mathrm{T}}^{\mathrm{miss}} > 100$ GeV. As in the previous

method, we require $M_T(\ell, E_T^{miss}) < 100$ GeV. The method has larger statistical power because the extractions are corrected with $p_T(W)$, thereby relaxing the requirement on the W boson decay from $E_T^{miss} > 200$ GeV to $E_T^{miss} > 100$ GeV. However, this method is more sensitive to larger systematic uncertainties due to the larger extrapolation between the control and search samples. The main assumption here is that the kinematics of the decay products of the W boson (i.e. the charged lepton and the neutrino) are similar between data and simulation. The dominant source of potential differences in the decay kinematics can be due to different fractions of the polarization components of the W boson between data and simulation. We assess uncertainties of up to 20% in the lost lepton background prediction to account for such effects. Other biases may arise due to differences in jet and E_T^{miss} resolution between data and simulation.

For both methods, we assess uncertainties in the simulation transfer factors due to possible differences between lepton selection efficiencies, b-tagging performance, and jet energy scale between data and simulation, and due to possible variations of the relative contributions of $t\bar{t}$ and W + jets processes. However, the dominant uncertainties associated with the background estimation are generally the consequence of the limited number of events present in the control regions, and in the simulated samples.

4.2 Estimation of the $Z \to \nu\nu$ background

An important source of background in the various search regions arises from events in which a Z boson, produced in association with jets, decays to neutrinos that result in a significant amount of missing energy in the event. The estimation of the $Z \to \nu\nu$ background combines information from Z+jets, with $Z \to \ell\ell$, and γ+jets samples. The former, referred to as the $Z \to \ell\ell$ sample, is used to measure the normalization of the $Z \to \nu\nu$ background in different ranges of N_b, while the much higher yields of the γ+jets sample are exploited to extract corrections to the search region variable distribution shapes. We obtain the $Z \to \ell\ell$ sample using dielectron and dimuon triggers. The leading lepton is required to have $p_T > 25(20)$ GeV while the trailing lepton must satisfy $p_T > 15(10)$ if they are electrons (muons). The γ+jets sample is collected by means of a single photon trigger and consists of events with photons with $p_T > 200$ GeV. The dilepton system or the photon momentum is added vectorially to $\vec{p}_T^{miss}$ in each event of the corresponding data samples. The modified E_T^{miss}, denoted by $E_T^{miss,\ell\ell}$ and $E_T^{miss,\gamma}$ for the $Z \to \ell\ell$ and γ+jets processes respectively, is used to calculate related kinematic variables.

The prediction of the $Z \to \nu\nu$ background is given by:

$$N_{Z\to\nu\nu}^{pred} = N_{Z\to\nu\nu}^{sim} \cdot R_Z \cdot S_\gamma \ , \tag{7}$$

where $N_{Z\to\nu\nu}^{sim}$ is the expected number of $Z \to \nu\nu$ events obtained from simulation, R_Z is a flavor dependent Z+jets normalization factor measured with the $Z \to \ell\ell$ sample and S_γ is a E_T^{miss} and jet kinematics shape correction factor extracted from the γ+jets sample.

The factor R_Z is calculated by comparing the observed and expected $Z \to \ell\ell$ yields after applying a relaxed version of the baseline selection. In particular, we remove the requirements on the azimuthal angles between jets and E_T^{miss} after confirming that this does not bias the result. To increase the purity of the $Z \to \ell\ell$ sample, we require the dilepton invariant mass to lie within the Z boson mass window: $80 < M_{\ell\ell} < 100$ GeV. The normalization of the non-negligible $t\bar{t}$ contamination is estimated in the region outside the Z boson mass window ($20 < M_{\ell\ell} < 80$ or $M_{\ell\ell} > 100$ GeV) and taken into account. Small contributions from tZ and $t\bar{t}Z$ processes are included in the $Z \to \ell\ell$ sample, and contributions from tW and $t\bar{t}W$ in the sample outside the Z boson mass window. To account for potential effects related to heavy flavor production, we calculate R_Z separately for different N_b requirements. The results are summarized in Table 3.

The uncertainty in R_Z due to the limited event counts in data and simulation ranges from 1% (for $N_b = 0$ in the low Δm analysis) to 14% (for $N_b \geq 2$ in the high Δm analysis).

Table 3: The R_Z factors obtained from $Z \to \ell\ell$+jets events that are used to normalize the $Z \to \nu\nu$ simulation sample. The factors are obtained using 12.9 fb^{-1} of data and calculated for different N_b selections in order to account for differences in heavy flavor production between data and simulation.

High Δm search		Low Δm search		
$N_b = 1$	$N_b \geq 2$	$N_b = 0$	$N_b \geq 1, N_b^L = 1$	$N_b \geq 1, N_b^L \geq 2$
1.06 ± 0.08	1.00 ± 0.14	0.97 ± 0.01	1.06 ± 0.07	1.07 ± 0.11

The quantity S_γ is the shape correction factor related to the modeling of the kinematics of $Z \to \nu\nu$ events. It is calculated via a comparison of the $E_T^{miss,\gamma}$ distributions of γ+jets events in simulation and data. The simulation is normalized to the number of events seen in data after applying the baseline selection. In order to suppress potential signal contamination and select a sample that is orthogonal to the search sample, we only consider events with $E_T^{miss} < 200\,GeV$ (here E_T^{miss} is the magnitude of the original $\vec{p}_T^{miss}$). The S_γ factor is estimated separately for each search region to account for any potential mismodeling of the search region observables in simulation. Since no statistically significant dependence of $E_T^{miss,\gamma}$ on N_b is observed, we integrate the γ+jets sample over N_b to improve the statistical power of the correction in the case of the high Δm analysis. For the low Δm analysis, we reduce the statistical uncertainties associated with S_γ by defining the zero-, and at least one b-tagged control regions using the loose CSV working point.

An assumption of the hybrid estimation method is that the shape differences between data and simulation are similar for $Z \to \nu\nu$ and photon events. This assumption is tested by comparing the ratios of data to simulation in the $Z \to \ell\ell$+jets process and the same ratio in the γ+jets process. We perform this comparison in different regions of N_b and across E_T^{miss} and any differences observed are assigned as systematic uncertainties in the $Z \to \nu\nu$ estimation. These uncertainties are expected to account for residual effects related to differences in the object description between data and simulation, as well as the absence of higher order corrections in the simulation of the two processes. The uncertainties range from 1% to 25%.

The γ+jets data control sample has contributions from three main components: prompt photons produced directly, via fragmentation, and fake photons, and may also contain sizable contributions (generally less than 10%, but up to 40% in regions with $N_t \geq 1, N_W \geq 1$, and large $E_T^{miss,\gamma}$) from the $t\bar{t}\gamma$ process in control regions corresponding to the high Δm analysis. The statistical uncertainty in the γ+jets data control sample and the uncertainty in R_Z are the major sources of uncertainty in the $Z \to \nu\nu$ prediction. The statistical uncertainty in the simulated samples, ranging up to about 40% in both the search regions and the γ+jets control regions, also has an important contribution. Uncertainties due to differences in the jet energy scale or b-tagging efficiency between data and simulation have a much smaller effect (less than 20%) on the $Z \to \nu\nu$ prediction.

4.3 Estimation of the QCD multijet background

The background originating from QCD multijet processes generally constitutes less than 20% of the total SM background in the search regions. It is estimated using a data control sample selected using the same trigger as for the search sample and enriched in QCD multijet events by inverting some of the requirements on the azimuthal angles between jets and E_T^{miss} that are

applied in the search region selection, namely by requiring $\Delta\phi_{123} < 0.1$ After correcting for the estimated contribution of other SM processes, we translate the observation in this control sample to a prediction in the search sample by means of transfer factors obtained from simulation. In general, the QCD multijet control regions are defined by applying the same set of selection criteria as applied in the search sample. Each transfer factor is defined as the ratio of the expected QCD multijet events in the signal region to the expected QCD multijet events in the control region. The estimation is carried out in each search region. For the high Δm search, since the shapes of key observables show little dependence on N_b, the QCD control sample is integrated over N_b to improve the statistical precision of the estimation. In regions with one or more top or W tags, we reduce the uncertainty in the prediction by integrating one or more E_T^{miss} regions in the control sample; a systematic uncertainty for this extrapolation is assigned by comparing the E_T^{miss} shapes in simulation and data for corresponding control regions that do not require the presence of top- or W-tagged candidates. Similarly, in the low Δm search, we combine E_T^{miss} bins in the QCD multijet control sample for the control regions defined with $N_b \geq 1$ and assign an uncertainty on the integration based on the data-to-simulation ratios observed in the $N_b = 0$ control regions.

The dominant uncertainties in the QCD multijet background estimation are still the result of the limited event yields in the control regions, the uncertainty assigned due to the integration in E_T^{miss}, and the statistical uncertainty in the transfer factors obtained from simulation.

4.4 Estimation of the rare SM backgrounds

Contributions from the $t\bar{t}Z$ process are generally small since this is a relatively rare process. However, it has a final state very similar to that of signal when the Z boson decays to neutrinos and both top quarks decay hadronically, and can constitute up to 25% of the total SM background in some search regions that require large E_T^{miss} and $N_t \geq 1$ or $N_W \geq 1$. Contributions from diboson processes (WW, WZ and ZZ) can contribute up to 10% of the total background in the $N_b = 0$ search regions. These backgrounds are predicted with NLO simulation and a 30% systematic uncertainty, obtained from 8 TeV CMS measurements [24], is assigned to the theoretical cross sections. Additional theoretical and experimental uncertainties in the prediction range up to 25% and 20% respectively, depending on the search region. We also take into consideration the statistical uncertainty of the simulation sample, which ranges from 5% up to 100% for regions with low contributions from these processes.

5 Results

Figures 4-5 and 6 show the observed events in each of the high Δm and low Δm search regions respectively, as well as the predicted SM background yields based on the background estimation methods discussed in Section 4. The predicted SM background yields and observed events in each search region are also tabulated in Tables 4 and 5 for the high Δm search and in Table 6 for the low Δm search. In general, the observed data agree well with the SM background predictions. The two search regions with the most significant discrepancies between the observed data and the predicted background correspond to the selection criteria $M_T(b_{1,2}, E_T^{miss}) > 175$ GeV, $N_b = 1, N_t \geq 1, N_W = 0, E_T^{miss} \in [450, 550)$ GeV, and $M_T(b_{1,2}, E_T^{miss}) > 175$ GeV, $N_b \geq 2, N_t \geq 1, N_W = 0, E_T^{miss} \in [350, 450)$ GeV for the high Δm analysis. In each of these search regions, the observed excess of events above the expected SM background corresponds to a local significance of ~ 1.9 standard deviations.

To allow an easier reintepretation of the results in the context of other models, we define aggregated regions defined by the combination of individual search regions. These results are

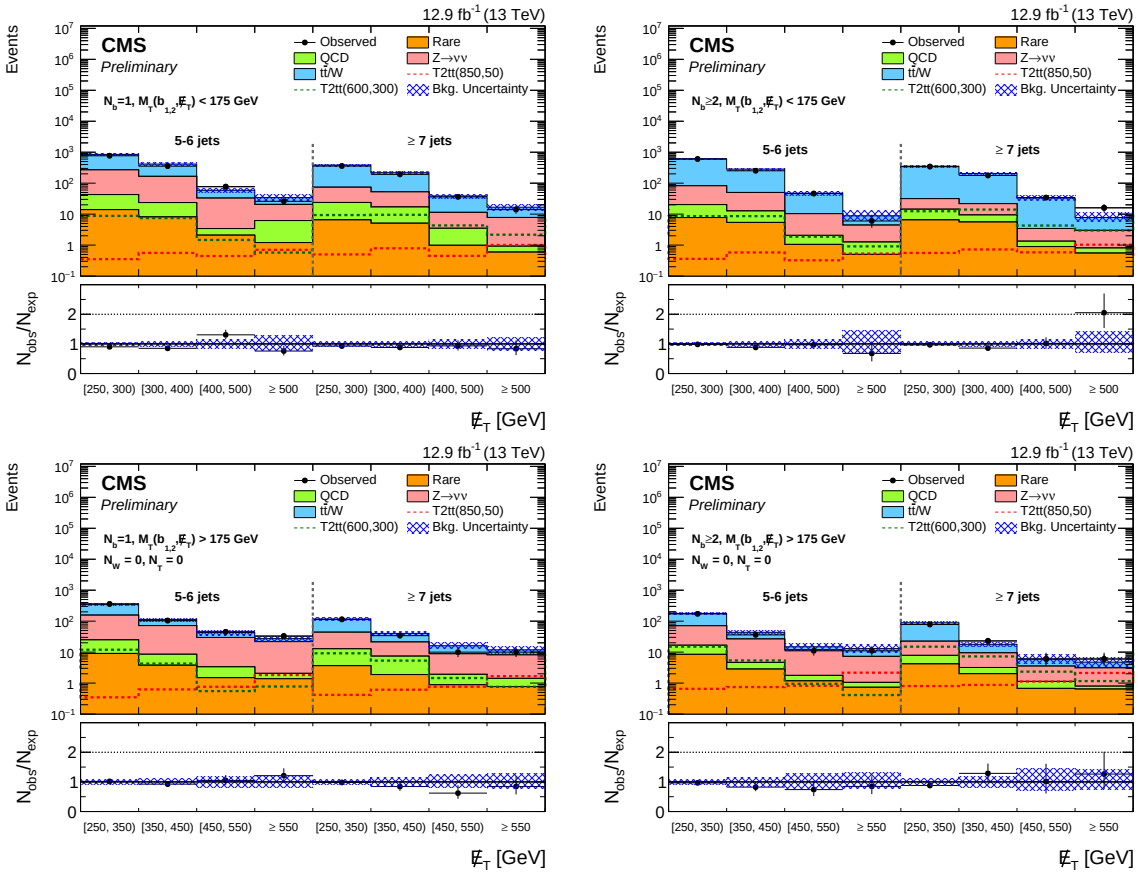

Figure 4: Observed events and SM estimates for the high Δm search regions with $M_{\mathrm{T}}(\mathrm{b}_{1,2}, E_{\mathrm{T}}^{\mathrm{miss}}) < 175$ GeV (top) and $M_{\mathrm{T}}(\mathrm{b}_{1,2}, E_{\mathrm{T}}^{\mathrm{miss}}) > 175$ GeV, $N_{\mathrm{t}} = 0, N_{\mathrm{W}} = 0$ (bottom), for events with $N_{\mathrm{b}} = 1$ (left) and $N_{\mathrm{b}} \geq 2$ (right). The SM background predictions shown do not include the effects of the maximum likelihood fit to the data. The ratio of the observed data to the SM prediction (black points, with error bars corresponding to the data statistical uncertainty) are shown in the ratio plots. The shaded blue band represents the statistical and systematic uncertainty on the background prediction.

presented in Appendix A.

Table 4: Predicted yields for each background with uncertainties in the $M_{\mathrm{T}}(\mathrm{b}_{1,2}, E_{\mathrm{T}}^{\mathrm{miss}}) < 175$ GeV regions of the high Δm search. The number of events observed in data is given in the last column.

Search region	$E_{\mathrm{T}}^{\mathrm{miss}}$ [GeV]	Lost lepton	$\mathrm{Z} \to \nu\nu$	Rare SM	QCD	Total SM	Observed
$N_{\mathrm{b}} = 1$, $M_{\mathrm{T}}(\mathrm{b}_{1,2}, E_{\mathrm{T}}^{\mathrm{miss}}) < 175$ GeV, $5 \leq N_{\mathrm{j}} < 7$							
0	250−300	581 ± 39	226 ± 25	14 ± 4	29 ± 10	849 ± 50	766
1	300−400	249 ± 23	142 ± 19	8.1 ± 2.6	16 ± 7	415 ± 34	353
2	400−500	26 ± 6	29 ± 7	2.1 ± 0.7	1.3 ± 0.6	59 ± 9	77
3	> 500	14^{+7}_{-5}	14 ± 3	1.2 ± 0.6	5.0 ± 5.5	34^{+10}_{-8}	26
$N_{\mathrm{b}} = 1$, $M_{\mathrm{T}}(\mathrm{b}_{1,2}, E_{\mathrm{T}}^{\mathrm{miss}}) < 175$ GeV, $N_{\mathrm{j}} \geq 7$							
4	250−300	310 ± 25	50 ± 7	6.5 ± 2.2	17 ± 4	384 ± 28	356
5	300−400	166 ± 16	35 ± 6	5.1 ± 1.7	12 ± 5	218 ± 18	192
6	400−500	27 ± 5	7.9 ± 2.3	0.98 ± 0.43	2.5 ± 1.1	39 ± 6	36
7	> 500	8.9 ± 2.9	6.9 ± 2.0	0.59 ± 0.28	0.33 ± 0.2	17 ± 4	14
$N_{\mathrm{b}} \geq 2$, $M_{\mathrm{T}}(\mathrm{b}_{1,2}, E_{\mathrm{T}}^{\mathrm{miss}}) < 175$ GeV, $5 \leq N_{\mathrm{j}} < 7$							
8	250−300	528 ± 34	62 ± 10	7.7 ± 2.5	13 ± 4	610 ± 37	600
9	300−400	234 ± 19	37 ± 7	5.4 ± 1.7	7.2 ± 2.4	284 ± 21	251
10	400−500	37 ± 7	8.3 ± 2.3	1.1 ± 0.4	1.0 ± 1.0	47 ± 7	46
11	> 500	$4.4^{+3.6}_{-2.2}$	3.2 ± 0.9	0.5 ± 0.22	0.75 ± 0.76	$8.8^{+3.9}_{-2.5}$	6
$N_{\mathrm{b}} \geq 2$, $M_{\mathrm{T}}(\mathrm{b}_{1,2}, E_{\mathrm{T}}^{\mathrm{miss}}) < 175$ GeV, $N_{\mathrm{j}} \geq 7$							
12	250−300	321 ± 23	17 ± 4	6.5 ± 2.1	7.9 ± 1.9	353 ± 24	342
13	300−400	184 ± 15	12 ± 2	5.6 ± 1.8	3.8 ± 1.1	206 ± 16	177
14	400−500	30 ± 5	2.1 ± 0.7	0.9 ± 0.42	0.44 ± 0.2	33 ± 5	34
15	> 500	$4.8^{+3.0}_{-2.0}$	2.2 ± 0.7	0.55 ± 0.24	0.25 ± 0.19	$7.8^{+3.2}_{-2.2}$	16

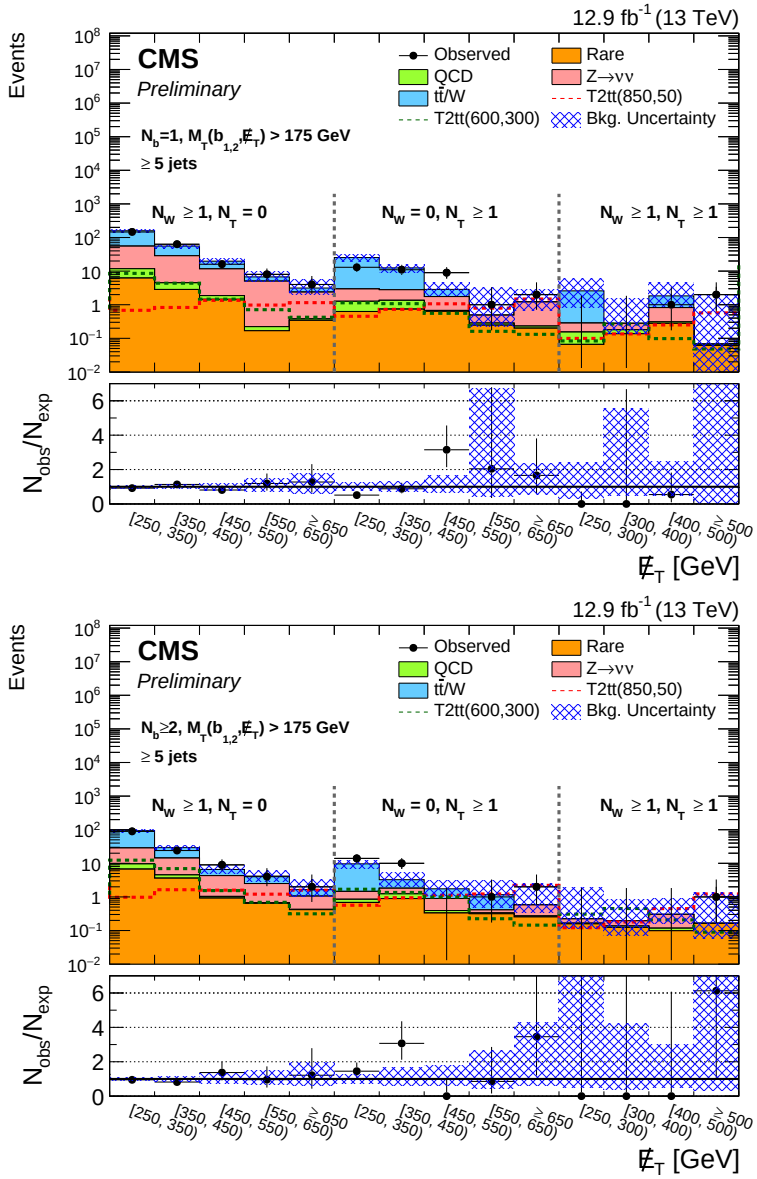

Figure 5: Observed events and SM estimates for the high Δm search regions with $M_{\mathrm{T}}(\mathrm{b}_{1,2}, E_{\mathrm{T}}^{\mathrm{miss}}) > 175$ GeV, $N_{\mathrm{j}} \geq 5$, and at least one top- or W-tagged candidate for events with $N_{\mathrm{b}} = 1$ (top) and $N_{\mathrm{b}} \geq 2$ (bottom). The SM background predictions shown do not include the effects of the maximum likelihood fit to the data. The ratio of the observed data to the SM prediction (black points, with error bars corresponding to the data statistical uncertainty) are shown in the ratio plots. The shaded blue band represents the statistical and systematic uncertainty on the background prediction.

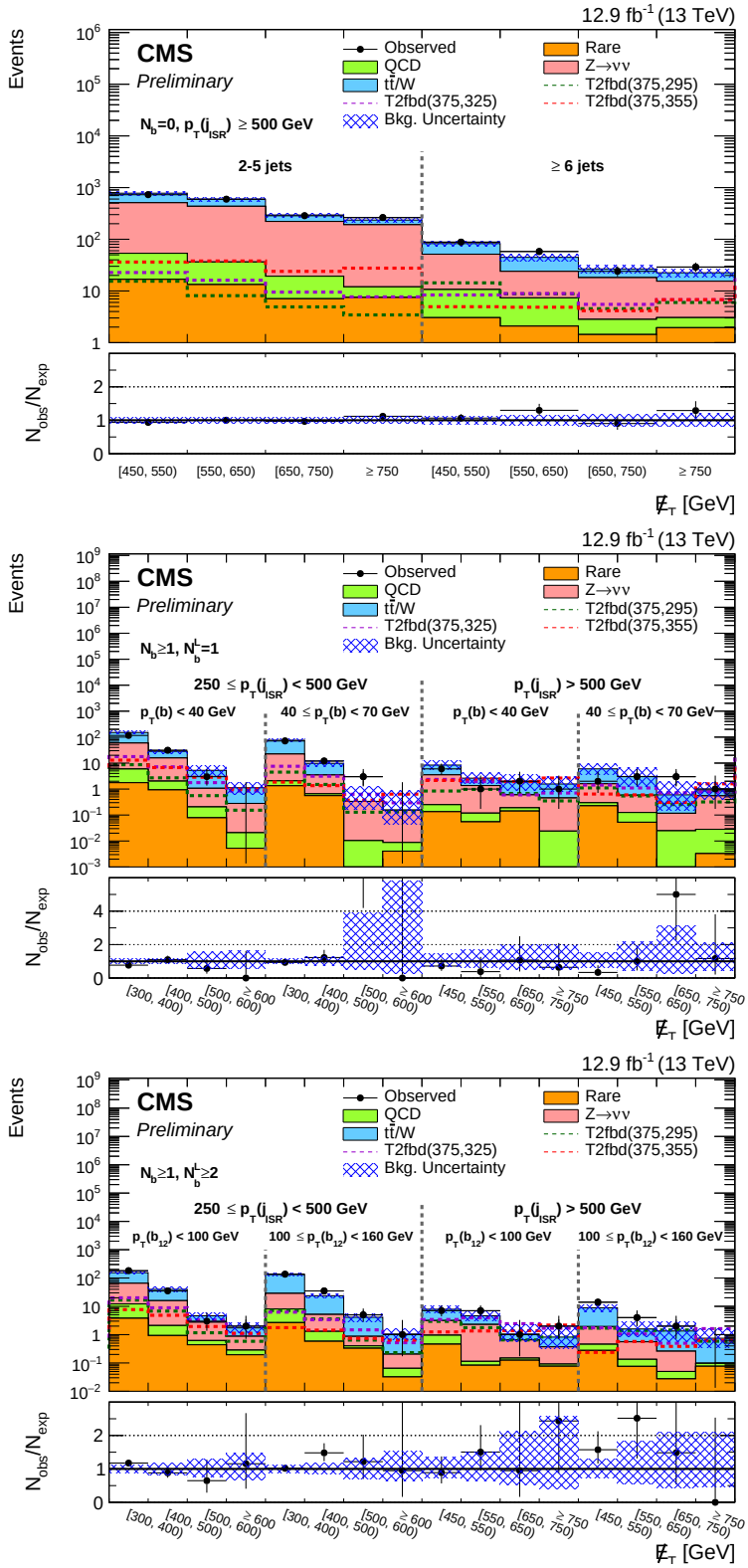

Figure 6: Observed events and SM estimates for the low Δm search regions. The SM background predictions shown do not include the effects of the maximum likelihood fit to the data. The ratio of the observed data to the SM prediction (black points, with error bars corresponding to the data statistical uncertainty) is shown in the ratio plots. The shaded blue band represents the statistical and systematic uncertainty on the background prediction. Top: for $N_{\mathrm{b}} = 0$; Middle: for $N_{\mathrm{b}} = 1$; Bottom: for $N_{\mathrm{b}} \geq 2$.

Table 5: Predicted yields for each background with uncertainties in the $M_T(b_{1,2}, E_T^{miss}) > 175$ GeV regions of the high Δm search. The number of events observed in data is given in the last column.

Search region	E_T^{miss} [GeV]	Lost lepton	$Z \to \nu\nu$	Rare SM	QCD	Total SM	Observed
$N_b = 1$, $M_T(b_{1,2}, E_T^{miss}) > 175$ GeV, $5 \le N_j < 7$, $N_t = 0$, $N_W = 0$							
16	250–350	195 ± 18	131 ± 15	9.1 ± 3.0	16 ± 4	351 ± 26	357
17	350–450	41 ± 7	63 ± 9	3.8 ± 1.3	4.7 ± 1.2	113 ± 12	104
18	450–550	13 ± 4	26 ± 6	1.5 ± 0.6	1.8 ± 0.8	43 ± 8	45
19	> 550	$5.5^{+3.4}_{-2.3}$	20 ± 4	1.4 ± 0.5	0.68 ± 0.39	27^{+6}_{-5}	33
$N_b = 1$, $M_T(b_{1,2}, E_T^{miss}) > 175$ GeV, $N_j \ge 7$, $N_t = 0$, $N_W = 0$							
20	250–350	72 ± 9	31 ± 5	3.6 ± 1.3	9.1 ± 2.5	116 ± 11	114
21	350–450	19 ± 4	14 ± 3	1.9 ± 0.7	5.5 ± 2.9	40 ± 6	34
22	450–550	$7.3^{+3.3}_{-2.5}$	6.9 ± 2.1	0.88 ± 0.37	1.0 ± 0.5	16^{+4}_{-3}	10
23	> 550	$3.7^{+2.4}_{-1.6}$	6.7 ± 1.8	0.77 ± 0.34	$0.65^{+0.57}_{-0.43}$	12^{+3}_{-2}	10
$N_b = 1$, $M_T(b_{1,2}, E_T^{miss}) > 175$ GeV, $N_j \ge 5$, $N_t = 0$, $N_W \ge 1$							
24	250–350	103 ± 12	44 ± 6	6.2 ± 2.0	5.6 ± 5.8	159 ± 15	146
25	350–450	27 ± 5	24 ± 4	2.8 ± 1.0	1.7 ± 1.8	56 ± 7	63
26	450–550	8.1 ± 2.7	9.8 ± 2.7	1.4 ± 0.5	$0.42^{+0.34}_{-0.3}$	20 ± 4	16
27	550–650	$1.7^{+2.4}_{-1.2}$	4.8 ± 1.5	0.17 ± 0.14	$0.05^{+0.14}_{-0.05}$	$6.7^{+3.0}_{-2.0}$	8
28	> 650	$0.76^{+1.78}_{-0.64}$	$2.0^{+1.2}_{-0.9}$	0.34 ± 0.15	$0.03^{+0.1}_{-0.04}$	$3.1^{+2.5}_{-1.2}$	4
$N_b = 1$, $M_T(b_{1,2}, E_T^{miss}) > 175$ GeV, $N_j \ge 5$, $N_t \ge 1$, $N_W = 0$							
29	250–350	22 ± 5	1.7 ± 0.6	0.63 ± 0.27	0.63 ± 0.7	25 ± 6	13
30	350–450	9.7 ± 3.3	$1.4^{+0.8}_{-0.6}$	0.74 ± 0.3	0.61 ± 0.74	12^{+4}_{-3}	11
31	450–550	$1.1^{+1.5}_{-0.8}$	$1.1^{+0.7}_{-0.5}$	0.64 ± 0.28	$0.04^{+0.05}_{-0.03}$	$2.9^{+1.8}_{-1.0}$	9
32	550–650	<2.49	$0.21^{+0.48}_{-0.17}$	0.25 ± 0.19	$0.04^{+0.1}_{-0.04}$	$0.49^{+2.79}_{-0.27}$	1
33	> 650	<1.07	$0.97^{+0.81}_{-0.51}$	0.2 ± 0.12	$0.03^{+0.08}_{-0.03}$	$1.2^{+1.7}_{-0.5}$	2
$N_b = 1$, $M_T(b_{1,2}, E_T^{miss}) > 175$ GeV, $N_j \ge 5$, $N_t \ge 1$, $N_W \ge 1$							
34	250–300	$2.3^{+3.5}_{-1.7}$	$0.13^{+0.2}_{-0.1}$	0.07 ± 0.06	$0.09^{+0.11}_{-0.09}$	$2.6^{+3.6}_{-1.7}$	0
35	300–400	<1.12	$0.1^{+0.24}_{-0.09}$	0.14 ± 0.1	$0.04^{+0.04}_{-0.03}$	$0.28^{+1.27}_{-0.14}$	0
36	400–500	$1.0^{+2.5}_{-0.9}$	$0.51^{+0.4}_{-0.27}$	0.28 ± 0.12	$0.03^{+0.04}_{-0.03}$	$1.8^{+2.6}_{-1.0}$	1
37	> 500	<1.61	<0.27	0.06 ± 0.07	0.01 ± 0.01	$0.07^{+1.78}_{-0.11}$	2
$N_b \ge 2$, $M_T(b_{1,2}, E_T^{miss}) > 175$ GeV, $5 \le N_j < 7$, $N_t = 0$, $N_W = 0$							
38	250–350	107 ± 12	54 ± 9	8.5 ± 2.7	8.2 ± 2.3	178 ± 16	172
39	350–450	17 ± 4	22 ± 4	2.8 ± 0.9	1.8 ± 0.6	44 ± 6	36
40	450–550	$3.0^{+3.0}_{-1.7}$	10 ± 3	1.2 ± 0.4	0.6 ± 0.29	15^{+4}_{-3}	11
41	> 550	$5.7^{+3.6}_{-2.4}$	6.2 ± 1.6	0.73 ± 0.28	0.32 ± 0.15	13^{+4}_{-3}	11
$N_b \ge 2$, $M_T(b_{1,2}, E_T^{miss}) > 175$ GeV, $N_j \ge 7$, $N_t = 0$, $N_W = 0$							
42	250–350	66 ± 9	15 ± 3	4.2 ± 1.4	3.7 ± 1.0	89 ± 10	78
43	350–450	8.4 ± 2.6	6.3 ± 1.6	2.0 ± 0.7	1.2 ± 0.4	18 ± 3	23
44	450–550	$2.4^{+2.4}_{-1.4}$	2.4 ± 0.8	0.67 ± 0.29	0.46 ± 0.22	$5.9^{+2.6}_{-1.7}$	6
45	> 550	$1.6^{+1.7}_{-1.0}$	2.3 ± 0.7	0.64 ± 0.25	$0.15^{+0.13}_{-0.1}$	$4.7^{+1.9}_{-1.2}$	6
$N_b \ge 2$, $M_T(b_{1,2}, E_T^{miss}) > 175$ GeV, $N_j \ge 5$, $N_t = 0$, $N_W \ge 1$							
46	250–350	65 ± 8	19 ± 3	6.7 ± 2.1	2.9 ± 3.1	94 ± 10	89
47	350–450	15 ± 4	9.8 ± 2.1	3.6 ± 1.2	0.9 ± 1.0	29 ± 5	24
48	450–550	$2.3^{+1.6}_{-1.1}$	3.3 ± 1.0	0.92 ± 0.36	$0.11^{+0.1}_{-0.09}$	$6.6^{+2.1}_{-1.6}$	9
49	550–650	$1.7^{+1.8}_{-1.0}$	1.8 ± 0.6	0.64 ± 0.25	$0.02^{+0.07}_{-0.02}$	$4.2^{+2.0}_{-1.3}$	4
50	> 650	$0.59^{+1.39}_{-0.5}$	$0.63^{+0.39}_{-0.28}$	0.42 ± 0.22	$0.01^{+0.02}_{-0.01}$	$1.6^{+1.6}_{-0.6}$	2
$N_b \ge 2$, $M_T(b_{1,2}, E_T^{miss}) > 175$ GeV, $N_j \ge 5$, $N_t \ge 1$, $N_W = 0$							
51	250–350	8.2 ± 2.7	0.61 ± 0.21	0.68 ± 0.27	0.17 ± 0.19	9.6 ± 2.7	14
52	350–450	$1.4^{+2.0}_{-1.0}$	$0.58^{+0.31}_{-0.23}$	0.89 ± 0.34	0.34 ± 0.51	$3.3^{+2.1}_{-1.2}$	10
53	450–550	$0.85^{+1.17}_{-0.58}$	$0.5^{+0.33}_{-0.24}$	0.33 ± 0.18	$0.06^{+0.09}_{-0.06}$	$1.7^{+1.3}_{-0.7}$	0
54	550–650	$0.76^{+1.79}_{-0.64}$	$0.08^{+0.18}_{-0.07}$	0.32 ± 0.19	$0.02^{+0.05}_{-0.02}$	$1.2^{+1.9}_{-0.7}$	1
55	> 650	<1.76	$0.31^{+0.26}_{-0.17}$	0.25 ± 0.15	$0.02^{+0.05}_{-0.02}$	$0.58^{+1.89}_{-0.23}$	2
$N_b \ge 2$, $M_T(b_{1,2}, E_T^{miss}) > 175$ GeV, $N_j \ge 5$, $N_t \ge 1$, $N_W \ge 1$							
56	250–300	<1.61	$0.06^{+0.09}_{-0.04}$	0.16 ± 0.1	0.01 ± 0.01	$0.22^{+1.65}_{-0.11}$	0
57	300–400	<0.53	$0.06^{+0.14}_{-0.05}$	0.12 ± 0.1	0.01 ± 0.01	$0.19^{+0.63}_{-0.12}$	0
58	400–500	<0.51	$0.19^{+0.15}_{-0.11}$	0.1 ± 0.09	0.02 ± 0.02	$0.3^{+0.6}_{-0.14}$	0
59	> 500	<1.08	<0.16	0.16 ± 0.1	<0.01	$0.16^{+1.19}_{-0.11}$	1

Table 6: Predicted yields for each background with uncertainties in the low Δm search regions. The number of events observed in data is given in the last column.

Search region	$E_{\mathrm{T}}^{\mathrm{miss}}$ [GeV]	Lost lepton	$\mathrm{Z} \to \nu\nu$	Rare SM	QCD	Total SM	Observed
$N_{\mathrm{b}} = 0$, $p_{\mathrm{T}}(\mathrm{ISR}) \geq 500$ GeV, $2 \leq N_{\mathrm{j}} < 6$							
0	450−550	269 ± 40	456 ± 53	17 ± 5	37 ± 11	778 ± 72	728
1	550−650	159 ± 27	398 ± 35	13 ± 4	23 ± 14	594 ± 51	595
2	650−750	74 ± 14	202 ± 21	7.1 ± 2.2	12 ± 6	295 ± 27	285
3	> 750	44 ± 8	179 ± 21	7.5 ± 2.5	4.5 ± 3.4	235 ± 25	263
$N_{\mathrm{b}} = 0$, $p_{\mathrm{T}}(\mathrm{ISR}) \geq 500$ GeV, $N_{\mathrm{j}} \geq 6$							
4	450−550	31 ± 6	41 ± 7	3.0 ± 1.1	7.6 ± 2.7	83 ± 10	88
5	550−650	21 ± 4	17 ± 4	2.1 ± 0.8	5.3 ± 1.9	45 ± 6	58
6	650−750	8.5 ± 2.2	15 ± 4	1.4 ± 0.6	1.4 ± 0.6	27 ± 5	24
7	> 750	7.0 ± 1.8	12 ± 4	1.9 ± 0.8	$1.1^{+0.7}_{-0.6}$	22 ± 4	29
$N_{\mathrm{b}} \geq 1, N_{\mathrm{b}}^{L} = 1, 250 \leq p_{\mathrm{T}}(\mathrm{ISR}) < 500$ GeV, $20 \leq p_{\mathrm{T}}(\mathrm{b}) < 40$ GeV							
8	300−400	92 ± 18	53 ± 6	1.8 ± 0.6	4.2 ± 4.4	151 ± 20	116
9	400−500	13 ± 4	14 ± 2	0.93 ± 0.36	1.1 ± 0.7	28 ± 4	31
10	500−600	$4.2^{+2.9}_{-2.1}$	0.86 ± 0.35	0.08 ± 0.07	0.13 ± 0.1	$5.2^{+3.0}_{-2.2}$	3
11	> 600	$0.85^{+0.67}_{-0.47}$	$0.26^{+0.18}_{-0.14}$	0.01 ± 0.01	0.02 ± 0.01	$1.1^{+0.7}_{-0.5}$	0
$N_{\mathrm{b}} \geq 1, N_{\mathrm{b}}^{L} = 1, 250 \leq p_{\mathrm{T}}(\mathrm{ISR}) < 500$ GeV, $40 \leq p_{\mathrm{T}}(\mathrm{b}) < 70$ GeV							
12	300−400	54 ± 11	20 ± 3	1.3 ± 0.5	0.73 ± 0.66	76 ± 12	71
13	400−500	6.3 ± 2.5	2.8 ± 0.9	0.56 ± 0.3	0.1 ± 0.09	9.8 ± 2.7	12
14	500−600	<0.87	$0.32^{+0.21}_{-0.15}$	<0.01	0.01 ± 0.01	$0.33^{+0.96}_{-0.17}$	3
15	> 600	<0.63	$0.14^{+0.21}_{-0.11}$	<0.01	<0.01	$0.15^{+0.74}_{-0.11}$	0
$N_{\mathrm{b}} \geq 1, N_{\mathrm{b}}^{L} = 1, p_{\mathrm{T}}(\mathrm{ISR}) \geq 500$ GeV, $20 \leq p_{\mathrm{T}}(\mathrm{b}) < 40$ GeV							
16	450−550	$4.8^{+3.7}_{-2.5}$	3.3 ± 0.7	0.13 ± 0.14	$0.12^{+0.09}_{-0.08}$	$8.4^{+3.8}_{-2.6}$	6
17	550−650	$1.3^{+1.7}_{-0.9}$	1.2 ± 0.5	0.05 ± 0.04	$0.06^{+0.06}_{-0.05}$	$2.6^{+1.8}_{-1.0}$	1
18	650−750	$1.3^{+1.8}_{-0.9}$	$0.41^{+0.26}_{-0.2}$	0.14 ± 0.14	$0.05^{+0.04}_{-0.03}$	$1.9^{+1.9}_{-1.0}$	2
19	> 750	$1.1^{+1.5}_{-0.8}$	$0.43^{+0.23}_{-0.19}$	<0.01	0.02 ± 0.02	$1.6^{+1.6}_{-0.8}$	1
$N_{\mathrm{b}} \geq 1, N_{\mathrm{b}}^{L} = 1, p_{\mathrm{T}}(\mathrm{ISR}) \geq 500$ GeV, $40 \leq p_{\mathrm{T}}(\mathrm{b}) < 70$ GeV							
20	450−550	$4.4^{+3.2}_{-2.3}$	1.3 ± 0.4	0.23 ± 0.14	$0.07^{+0.08}_{-0.06}$	$6.0^{+3.2}_{-2.3}$	2
21	550−650	$2.5^{+3.5}_{-1.7}$	$0.45^{+0.32}_{-0.25}$	0.05 ± 0.07	$0.07^{+0.07}_{-0.05}$	$3.1^{+3.6}_{-1.8}$	3
22	650−750	$0.48^{+1.18}_{-0.44}$	$0.09^{+0.22}_{-0.08}$	<0.01	$0.02^{+0.03}_{-0.02}$	$0.6^{+1.29}_{-0.45}$	3
23	> 750	$0.31^{+0.76}_{-0.33}$	$0.52^{+0.41}_{-0.29}$	<0.01	$0.02^{+0.03}_{-0.02}$	$0.86^{+0.98}_{-0.46}$	1
$N_{\mathrm{b}} \geq 1, N_{\mathrm{b}}^{L} \geq 2, 250 \leq p_{\mathrm{T}}(\mathrm{ISR}) < 500$ GeV, $40 \leq p_{\mathrm{T}}(\mathrm{b})_1 + p_{\mathrm{T}}(\mathrm{b})_2 < 100$ GeV							
24	300−400	89 ± 16	53 ± 8	3.8 ± 1.3	8.4 ± 6.2	154 ± 19	181
25	400−500	24 ± 6	14 ± 3	0.93 ± 0.41	1.2 ± 0.6	40 ± 7	35
26	500−600	$1.9^{+1.0}_{-0.8}$	2.1 ± 0.8	0.44 ± 0.22	0.18 ± 0.1	$4.6^{+1.4}_{-1.1}$	3
27	> 600	$0.86^{+0.52}_{-0.4}$	$0.59^{+0.52}_{-0.35}$	0.19 ± 0.1	0.09 ± 0.06	$1.7^{+0.8}_{-0.6}$	2
$N_{\mathrm{b}} \geq 1, N_{\mathrm{b}}^{L} \geq 2, 250 \leq p_{\mathrm{T}}(\mathrm{ISR}) < 500$ GeV, $100 \leq p_{\mathrm{T}}(\mathrm{b})_1 + p_{\mathrm{T}}(\mathrm{b})_2 < 160$ GeV							
28	300−400	105 ± 13	21 ± 4	2.7 ± 0.9	5.4 ± 3.2	134 ± 15	136
29	400−500	18 ± 4	3.9 ± 1.1	0.58 ± 0.27	0.72 ± 0.43	24 ± 4	35
30	500−600	3.2 ± 1.2	$0.47^{+0.43}_{-0.27}$	0.33 ± 0.15	0.07 ± 0.04	$4.1^{+1.4}_{-1.3}$	5
31	> 600	0.85 ± 0.36	$0.14^{+0.33}_{-0.12}$	0.03 ± 0.04	0.03 ± 0.02	$1.1^{+0.5}_{-0.4}$	1
$N_{\mathrm{b}} \geq 1, N_{\mathrm{b}}^{L} \geq 2, p_{\mathrm{T}}(\mathrm{ISR}) \geq 500$ GeV, $40 \leq p_{\mathrm{T}}(\mathrm{b})_1 + p_{\mathrm{T}}(\mathrm{b})_2 < 100$ GeV							
32	450−550	$4.7^{+2.5}_{-1.9}$	2.2 ± 0.6	0.46 ± 0.21	$0.49^{+0.66}_{-0.43}$	$7.9^{+2.8}_{-2.1}$	7
33	550−650	$2.4^{+2.1}_{-1.4}$	2.2 ± 0.9	0.08 ± 0.05	$0.03^{+0.04}_{-0.02}$	$4.7^{+2.3}_{-1.6}$	7
34	650−750	$0.4^{+0.95}_{-0.35}$	$0.51^{+0.44}_{-0.29}$	0.12 ± 0.11	$0.02^{+0.03}_{-0.02}$	$1.1^{+1.2}_{-0.5}$	1
35	> 750	$0.45^{+1.1}_{-0.41}$	$0.28^{+0.39}_{-0.2}$	0.08 ± 0.06	$0.01^{+0.02}_{-0.01}$	$0.82^{+1.3}_{-0.49}$	2
$N_{\mathrm{b}} \geq 1, N_{\mathrm{b}}^{L} \geq 2, p_{\mathrm{T}}(\mathrm{ISR}) \geq 500$ GeV, $100 \leq p_{\mathrm{T}}(\mathrm{b})_1 + p_{\mathrm{T}}(\mathrm{b})_2 < 160$ GeV							
36	450−550	7.0 ± 2.4	$1.5^{+0.8}_{-0.6}$	0.28 ± 0.16	$0.18^{+0.2}_{-0.14}$	$8.9^{+2.7}_{-2.5}$	14
37	550−650	$1.0^{+1.1}_{-0.6}$	$0.42^{+0.47}_{-0.29}$	0.08 ± 0.11	$0.06^{+0.06}_{-0.04}$	$1.6^{+1.3}_{-0.7}$	4
38	650−750	$1.1^{+1.2}_{-0.7}$	$0.21^{+0.5}_{-0.19}$	0.03 ± 0.02	0.02 ± 0.02	$1.3^{+1.5}_{-0.8}$	2
39	> 750	$0.65^{+0.69}_{-0.41}$	<0.21	0.08 ± 0.05	0.02 ± 0.02	$0.75^{+0.83}_{-0.41}$	0

6 Interpretation

The statistical interpretation of the results in terms of exclusion limits for the signal models considered is based on a binned likelihood fit to the observed data taking into account the predicted background and signal yields in each bin. The extraction of exclusion limits is based on a modified frequentist approach [25]. All search region bins, as well as the corresponding single-lepton control region bins, are fit simultaneously in order to evaluate the cross section excluded at 95% confidence level for each signal benchmark point considered in each analysis. Signal models for which the 95% upper limit on the production cross section falls below the theoretical cross section (based on NLO+NLL calculations) are considered to be excluded by the analysis.

The inclusion of the single-lepton control region in the simultaneous fit ensures that any potential signal contamination in the control region, based on the corresponding estimated event yields for any given signal model, is taken into account in the signal strength excluded by the maximum likelihood fit. The systematic uncertainties assigned to the signal and background predictions are treated as nuisance parameters in the fit. Statistical uncertainties due to the limited statistics of simulated samples are uncorrelated between all regions and for all backgrounds. The statistical uncertainties related to the data in control regions are correlated between search regions which derive their background prediction from the same control regions (e.g. across different N_b bins for a given data-driven background prediction). In the case of the lost lepton background, the statistical uncertainty of the data and the systematic uncertainty on the signal yield in each single-lepton control region bin are correlated to the corresponding uncertainties in the search region bins that derive their lost-lepton background prediction from this bin.

The experimental uncertainties related to the lepton and hadronic tau vetoes, b-tagging, jet energy scale, and pileup reweighting are correlated across all search regions and for all backgrounds. The uncertainties in the lost-lepton background estimate corresponding to the variations of its $t\bar{t}$ and W fractions respectively, of the W boson polarization, or of the E_T^{miss} resolution in simulation are also correlated for all search regions. The uncertainties assigned to the $Z \to \nu\nu$ prediction due to the uncertainties in R_Z and the discrepancies between the data-to-simulation ratios in $Z \to \ell\ell$+jets and γ+jets events are correlated separately for all regions with the same N_b. Uncertainties due to the lepton efficiency correction factors are treated as being anti-correlated between the single-lepton control region and the search region, since an underestimate of the efficiency for selecting leptons in the control region would result in an overestimate in the efficiency for vetoing leptons in the search region.

For the simulated signal event samples, differences between the fast simulation and the full GEANT4-based simulation are taken into account. Appropriate corrections and uncertainties for differences observed in the lepton selection efficiencies, b tagging performance, jet energy scale, and top and W tagging efficiencies are applied to the predicted signal yields. The modeling of initial-state radiation (ISR) plays an important role in cases where we rely on the $\tilde{t}_1\bar{\tilde{t}}_1$ system to have significant boost, such as for low Δm scenarios. Correction factors and uncertainties determined by comparing the simulated and observed ISR jet spectrum in dilepton $t\bar{t}$ events are applied to the signal based on the ISR jet multiplicity. We also assess uncertainties in the predicted signal yields due to variations of the renormalization and factorization scales in simulation. An extra correction and uncertainty is assigned for possible differences in E_T^{miss} resolution between the fast and full simulation models. This uncertainty is correlated between all search regions under the assumption of a uniform prior.

The results of the high Δm analysis are used to set exclusion limits in signal scenarios in which

the top squarks undergo one of the two decays: $\widetilde{t}_1 \to t\widetilde{\chi}_1^0$ or $\widetilde{t}_1 \to b\widetilde{\chi}_1^{\pm} \to bW^{\pm(*)}\widetilde{\chi}_1^0$. We consider two scenarios, one in which the top squarks decay solely through the $\widetilde{t}_1 \to t\widetilde{\chi}_1^0$ decay mode, and one in which they decay only via the $\widetilde{t}_1 \to b\widetilde{\chi}_1^{\pm}$ mode. In the decay via an intermediate chargino, the experimental signature is affected by the mass of the chargino. The mass configurations studied here are those in which the $\widetilde{\chi}_1^{\pm}$ mass is equidistant from the $\widetilde{t}_1$ and $\widetilde{\chi}_1^0$ masses.

Figure 7 shows the 95% CL exclusion limits obtained for simplified models in the pure $\widetilde{t}_1 \to t\widetilde{\chi}_1^0$ decay scenario. Using the 12.9 fb^{-1}dataset, we probe $\widetilde{t}_1$ masses up to 860 GeV, and $\widetilde{\chi}_1^0$ masses up to 320 GeV in this scenario. We do not perform an interpretation for values of Δm that are very close to the top quark mass when the $\widetilde{\chi}_1^0$ is very light. These signal topologies are particularly challenging due to their similarity to the SM $t\bar{t}$ background, resulting in a significant contamination from leptonic signal events in the search regions. Figure 8 shows the exclusion limits obtained in the pure $\widetilde{t}_1 \to b\widetilde{\chi}_1^{\pm}$ decay scenario. Under this decay hypothesis, we probe $\widetilde{t}_1$ masses up to 740 GeV, and $\widetilde{\chi}_1^0$ masses up to 260 GeV.

The results of the low Δm analysis are used to set exclusion limits in signal scenarios in which the mass difference between the $\widetilde{t}_1$ and $\widetilde{\chi}_1^0$ is smaller than the W boson mass. In these models the top squark is assumed to decay through an off-shell top quark and subsequently an off-shell W boson ($\widetilde{t}_1 \to t^*b, t^* \to W^{\pm *}\widetilde{\chi}_1^0, W^{\pm *} \to f\bar{f}$). The model used to interpret the current results represents a simplified version of the four body decay in which the top quark decay width is neglected. Figure 9 shows the 95% CL exclusion limits obtained for simplified models describing this scenario. Using the 12.9 fb^{-1}dataset, we probe $\widetilde{t}_1$ masses up to 450 GeV, and $\widetilde{\chi}_1^0$ masses up to 430 GeV in this scenario.

7 Summary

The results of a search for direct production of top squark pairs in the fully-hadronic final state have been presented, based on data collected in 2016 by the CMS detector in proton-proton collisions at a center-of-mass energy of 13 TeV. The data correspond to an integrated luminosity of 12.9 fb^{-1}. No significant excess of events beyond the expected contribution from standard model processes is observed, and exclusion limits are set in the context of simplified models of top squark production. Top squark masses up to 450 GeV are probed for a neutralino mass of 430 GeV in the scenario of a very compressed mass spectrum between the $\widetilde{t}_1$ and $\widetilde{\chi}_1^0$ where the $\widetilde{t}_1$ decays via a four body decay. In the scenario of larger mass differences between the $\widetilde{t}_1$ and $\widetilde{\chi}_1^0$ when the top squark decays to an on-shell top quark and a neutralino, top squark masses up to 860 GeV, and $\widetilde{\chi}_1^0$ masses up to 320 GeV are probed. When the top squarks decay to a bottom quark and a $\widetilde{\chi}_1^{\pm}$, top squark masses up to 740 GeV, and $\widetilde{\chi}_1^0$ masses up to 260 GeV are probed.

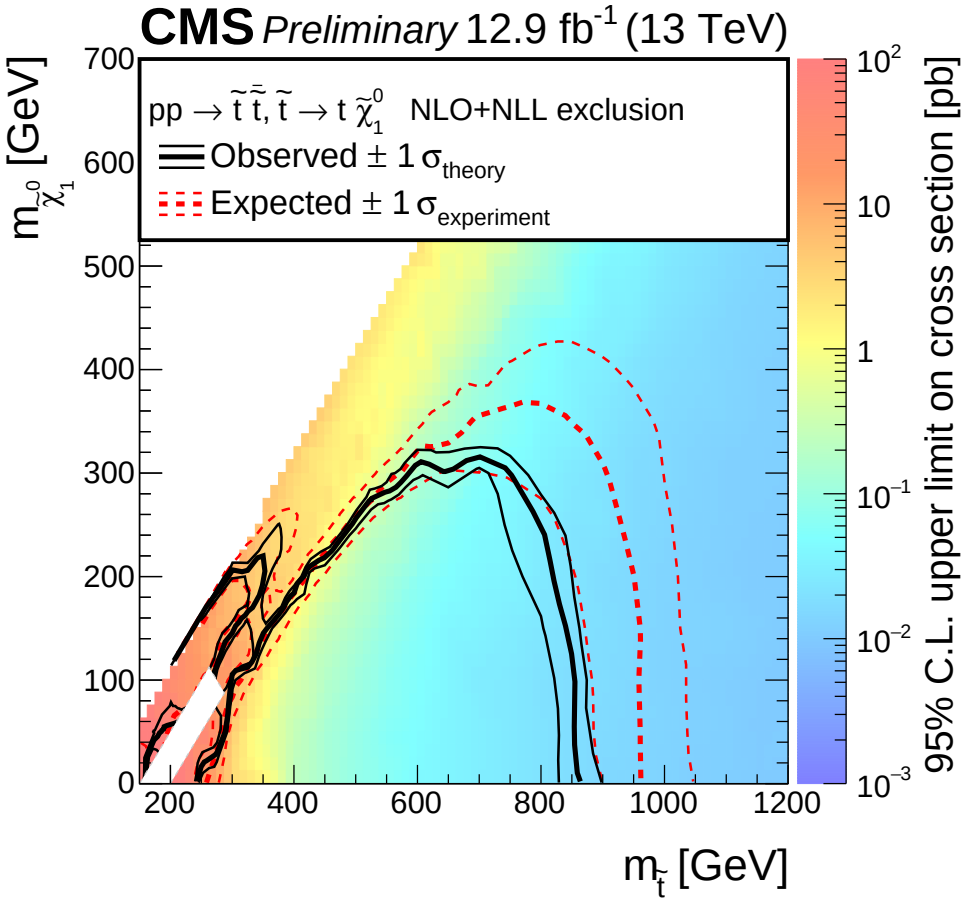

Figure 7: Exclusion limits at 95% CL for simplified models of top squark pair production in the pure $\tilde{t}_1 \to t\tilde{\chi}_1^0$ ("T2tt") decay scenario. The solid black curves represent the observed exclusion contours with respect to NLO+NLL cross section calculations [22] and the corresponding ± 1 standard deviations. The dashed red curves indicate the expected exclusion contour and the ± 1 standard deviations with experimental uncertainties.

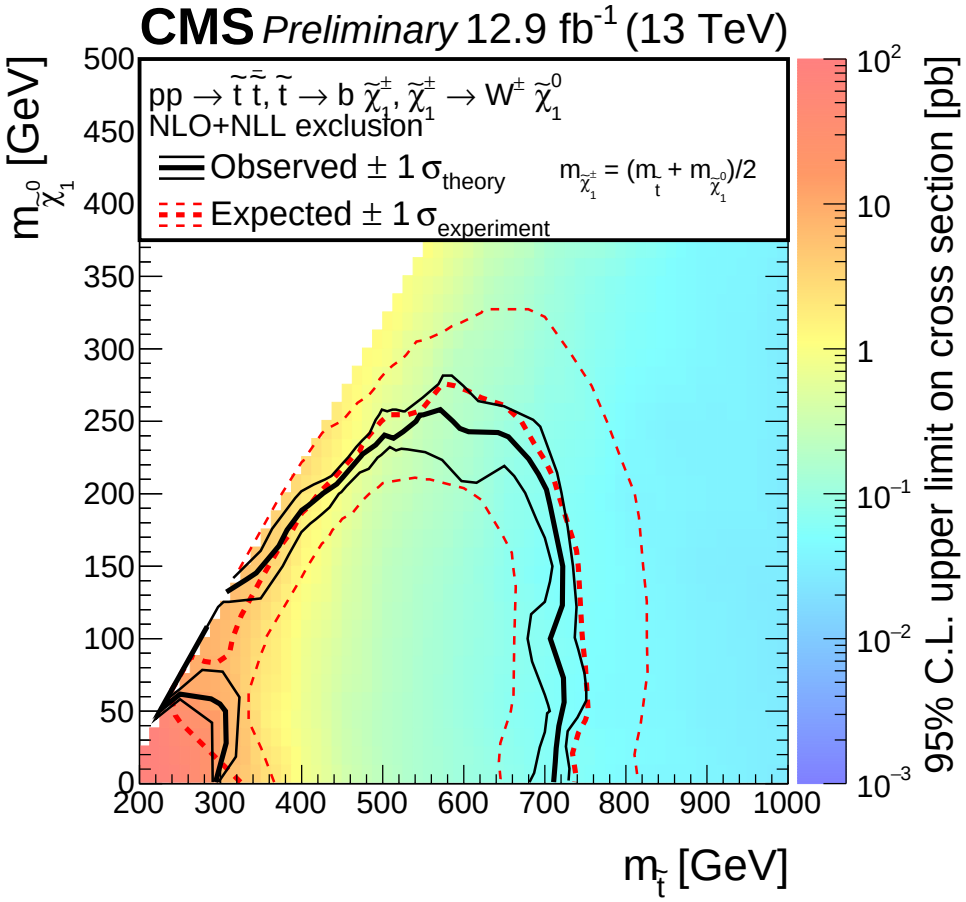

Figure 8: Exclusion limits at 95% CL for simplified models of top squark pair production in the pure $\tilde{t}_1 \rightarrow b\tilde{\chi}_1^{\pm} \rightarrow bW^{\pm(*)}\tilde{\chi}_1^0$ ("T2bW") decay scenario. The solid black curves represent the observed exclusion contours with respect to NLO+NLL cross section calculations [22] and the corresponding ± 1 standard deviations. The dashed red curves indicate the expected exclusion contour and the ± 1 standard deviations with experimental uncertainties.

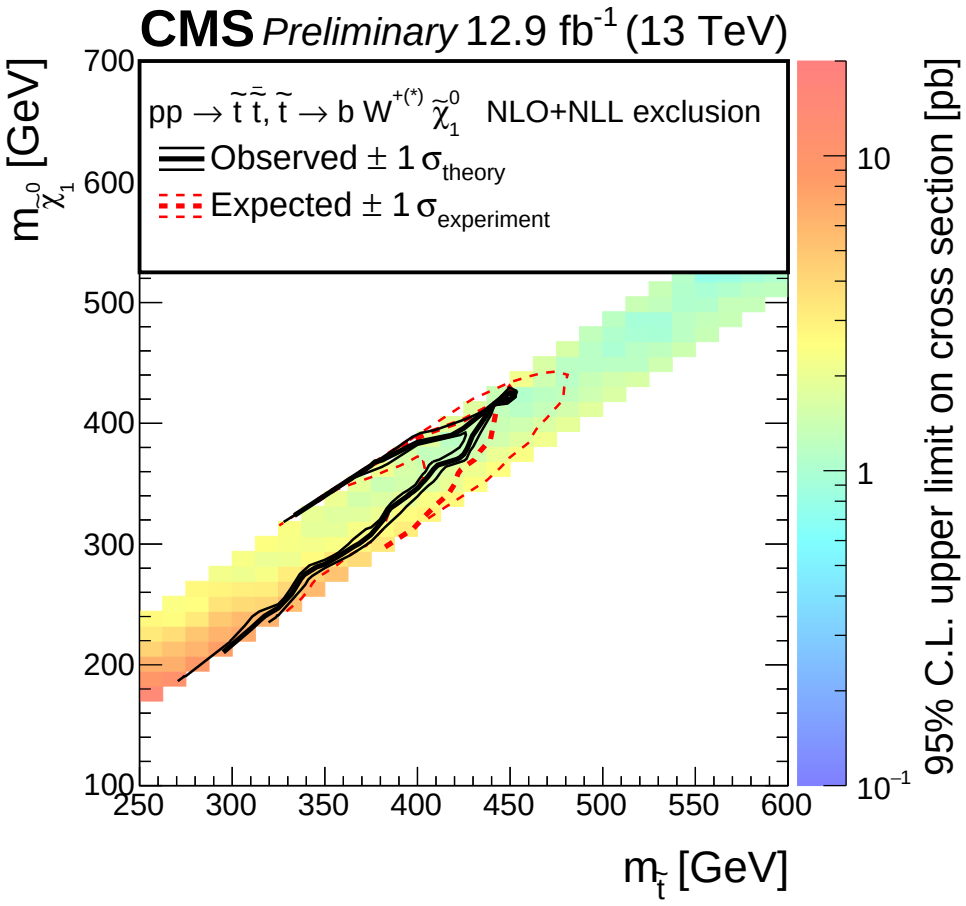

Figure 9: Exclusion limits at 95% CL for simplified models of top squark pair production in the $\tilde{t}_1 \rightarrow bf\bar{f}\tilde{\chi}_1^0$ ("T2fbd") four-body decay scenario. The solid black curves represent the observed exclusion contours with respect to NLO+NLL cross section calculations [22] and the corresponding ± 1 standard deviations. The dashed red curves indicate the expected exclusion contour and the ± 1 standard deviations with experimental uncertainties.

References

[1] CMS Collaboration, "Search for direct production of top squark pairs decaying to all-hadronic final states in pp collisions at sqrt(s) = 13 TeV", CMS Physics Analysis Summary CMS-PAS-SUS-16-007, 2016.

[2] C. Balazs, M. Carena, and C. E. M. Wagner, "Dark matter, light stops and electroweak baryogenesis", *Phys. Rev. D* **70** (2004) 015007, doi:10.1103/PhysRevD.70.015007, arXiv:hep-ph/0403224.

[3] CMS Collaboration, "Particle-Flow Event Reconstruction in CMS and Performance for Jets, Taus, and $E_{\mathrm{T}}^{\mathrm{miss}}$", CMS Physics Analysis Summary CMS-PAS-PFT-09-001, 2009.

[4] CMS Collaboration, "Commissioning of the Particle-flow Event Reconstruction with the first LHC collisions recorded in the CMS detector", CMS Physics Analysis Summary CMS-PAS-PFT-10-001, 2010.

[5] M. Cacciari, G. P. Salam, and G. Soyez, "The anti-k_t jet clustering algorithm", *JHEP* **04** (2008) 063, doi:10.1088/1126-6708/2008/04/063, arXiv:0802.1189.

[6] CMS Collaboration, "Identification of b-quark jets with the CMS experiment", *JINST* **8** (2013) P04013, doi:10.1088/1748-0221/8/04/P04013, arXiv:1211.4462.

[7] CMS Collaboration, "Performance of b tagging at $\sqrt{s} = 8$ TeV in multijet, $\mathrm{t\bar{t}}$ and boosted topology events", CMS Physics Analysis Summary CMS-PAS-BTV-13-001, 2013.

[8] CMS Collaboration, "Performance of electron reconstruction and selection with the CMS detector in proton-proton collisions at $\sqrt{s} = 8$ TeV", *JINST* **10** (2015) P06005, doi:10.1088/1748-0221/10/06/P06005, arXiv:1502.02701.

[9] CMS Collaboration, "Performance of CMS muon reconstruction in pp collision events at $\sqrt{s} = 7$ TeV", *JINST* **7** (2012) P10002, doi:10.1088/1748-0221/7/10/P10002, arXiv:1206.4071.

[10] A. J. Larkoski, S. Marzani, G. Soyez, and J. Thaler, "Soft Drop", *JHEP* **05** (2014) 146, doi:10.1007/JHEP05(2014)146, arXiv:1402.2657.

[11] J. Thaler and K. Van Tilburg, "Maximizing Boosted Top Identification by Minimizing N-subjettiness", *JHEP* **1202** (2012) 093, doi:10.1007/JHEP02(2012)093, arXiv:1108.2701.

[12] J. Alwall et al., "MadGraph5: going beyond", *JHEP* **06** (2011) 128, doi:10.1007/JHEP06(2011)128, arXiv:1106.0522.

[13] NNPDF Collaboration, "Parton distributions for the LHC Run II", *JHEP* **04** (2015) 040, doi:10.1007/JHEP04(2015)040, arXiv:1410.8849.

[14] P. Nason, "A New method for combining NLO QCD with shower Monte Carlo algorithms", *JHEP* **11** (2004) 040, doi:10.1088/1126-6708/2004/11/040, arXiv:hep-ph/0409146.

[15] S. Frixione, P. Nason, and C. Oleari, "Matching NLO QCD computations with Parton Shower simulations: the POWHEG method", *JHEP* **11** (2007) 070, doi:10.1088/1126-6708/2007/11/070, arXiv:0709.2092.

[16] S. Alioli, P. Nason, C. Oleari, and E. Re, "A general framework for implementing NLO calculations in shower Monte Carlo programs: the POWHEG BOX", *JHEP* **06** (2010) 043, doi:10.1007/JHEP06(2010)043, arXiv:1002.2581.

[17] E. Re, "Single-top Wt-channel production matched with parton showers using the POWHEG method", *Eur. Phys. J. C* **71** (2011) 1547, doi:10.1140/epjc/s10052-011-1547-z, arXiv:1009.2450.

[18] J. Alwall et al., "The automated computation of tree-level and next-to-leading order differential cross sections, and their matching to parton shower simulations", *JHEP* **07** (2014) 079, doi:10.1007/JHEP07(2014)079, arXiv:1405.0301.

[19] T. Sjostrand, S. Mrenna, and P. Z. Skands, "A Brief Introduction to PYTHIA 8.1", *Comput. Phys. Commun.* **178** (2008) 852–867, doi:10.1016/j.cpc.2008.01.036, arXiv:0710.3820.

[20] GEANT4 Collaboration, "GEANT4—a simulation toolkit", *Nucl. Instrum. Meth. A* **506** (2003) 250, doi:10.1016/S0168-9002(03)01368-8.

[21] S. Abdullin et al., "The fast simulation of the CMS detector at LHC", *J. Phys. Conf. Ser.* **331** (2011) 032049, doi:10.1088/1742-6596/331/3/032049.

[22] C. Borschensky et al., "Squark and gluino production cross sections in pp collisions at $\sqrt{s}$ = 13, 14, 33 and 100 TeV", *Eur. Phys. J. C* **74** (2014) 3174, doi:10.1140/epjc/s10052-014-3174-y, arXiv:1407.5066.

[23] CMS Collaboration, "Identification of b quark jets at the CMS Experiment in the LHC Run 2", CMS Physics Analysis Summary CMS-PAS-BTV-15-001, 2016.

[24] CMS Collaboration, "Observation of top quark pairs produced in association with a vector boson in pp collisions at $\sqrt{s} = 8$ TeV", *JHEP* **01** (2016) 096, doi:10.1007/JHEP01(2016)096, arXiv:1510.01131.

[25] ATLAS and CMS Collaborations, "Procedure for the LHC Higgs boson search combination in summer 2011", Technical Report ATL-PHYS-PUB-2011-011, CMS NOTE-2011/005, 2011.

A Aggregate search regions

We also define a set of aggregate search regions by combining groups of the full set of search regions. These aggregate regions represent a simplified version of the analysis and provide sensitivity to different signal topologies. Tables 7 and 8 describe the definitions of the aggregate regions. Figure 10 shows the observed events and the predicted background yields based on the background estimation methods discussed in Section 4 for each of these aggregate regions for the high Δm and low Δm analyses. The yields are also tabulated in Tables 9 and 10.

Table 7: Summary of the 13 disjoint aggregate search regions defined for the high Δm analysis.

Category	$M_{\mathrm{T}}(\mathrm{b}_{1,2}, E_{\mathrm{T}}^{\mathrm{miss}}) < 175$ GeV		$M_{\mathrm{T}}(\mathrm{b}_{1,2}, E_{\mathrm{T}}^{\mathrm{miss}}) \geq 175$ GeV			
$N_{\mathrm{t}}/N_{\mathrm{W}}$	$-$		$N_{\mathrm{t}}=0, N_{\mathrm{W}}=0$	$N_{\mathrm{t}}\geq 1, N_{\mathrm{W}}=0$	$N_{\mathrm{t}}=0, N_{\mathrm{W}}\geq 1$	$N_{\mathrm{t}}\geq 1, N_{\mathrm{W}}\geq 1$
N_{j}	≥ 7		≥ 7	≥ 5	≥ 5	≥ 5
N_{b}	1	≥ 2	≥ 2	≥ 2	≥ 2	≥ 2
$E_{\mathrm{T}}^{\mathrm{miss}}$ [GeV]	250−300 300−400	250−300 300−400	250−350 350−450 450−550 ≥550	250−450 >450	250−450 >450	>250

Table 8: Summary of the 12 disjoint aggregate search regions defined for the low Δm analysis.

Category	$N_{\mathrm{b}}\geq 1, N_{\mathrm{b}}^{L}=1$		$N_{\mathrm{b}}\geq 1, N_{\mathrm{b}}^{L}\geq 2$	
$p_{\mathrm{T}}(\mathrm{ISR})$	>250		>250	
$p_{\mathrm{T}}(\mathrm{b})$ or $p_{\mathrm{T}}(\mathrm{b}_{12})$	$20-40$	$40-70$	$40-100$	$100-160$
$E_{\mathrm{T}}^{\mathrm{miss}}$ [GeV]	300−400 400−500 >500	300−400 400−500 >500	300−400 400−500 >500	300−400 400−500 >500

Table 9: Observed events and SM estimates for the aggregate search regions of the high Δm analysis.

Search region	$E_{\mathrm{T}}^{\mathrm{miss}}$ [GeV]	Lost lepton	$\mathrm{Z}\to\nu\nu$	Rare SM	QCD	Total SM	Observed
$N_{\mathrm{b}}=1$, $M_{\mathrm{T}}(\mathrm{b}_{1,2}, E_{\mathrm{T}}^{\mathrm{miss}}) < 175$ GeV, $nj\geq 7$							
0	250−300	312 ± 25	48 ± 6	6.5 ± 3.4	17 ± 4	384 ± 28	356
1	300−400	167 ± 17	34 ± 5	5.1 ± 2.6	12 ± 5	218 ± 18	192
$N_{\mathrm{b}}\geq 2$, $M_{\mathrm{T}}(\mathrm{b}_{1,2}, E_{\mathrm{T}}^{\mathrm{miss}}) < 175$ GeV, $nj\geq 7$							
2	250−300	323 ± 23	17 ± 3	6.5 ± 3.3	7.9 ± 1.9	354 ± 25	342
3	300−400	186 ± 16	12 ± 2	5.6 ± 2.9	3.8 ± 1.1	207 ± 16	177
$N_{\mathrm{b}}\geq 2$, $M_{\mathrm{T}}(\mathrm{b}_{1,2}, E_{\mathrm{T}}^{\mathrm{miss}}) > 175$ GeV, $nj\geq 7$, $N_{\mathrm{t}}=0$, $N_{\mathrm{W}}=0$							
4	250−350	67 ± 9	14 ± 3	4.1 ± 2.2	3.7 ± 1.0	88 ± 10	78
5	350−450	8.4 ± 2.6	6.0 ± 1.4	2.0 ± 1.1	1.2 ± 0.4	18 ± 3	23
6	450−550	$2.4^{+2.4}_{-1.4}$	2.3 ± 0.7	0.67 ± 0.4	0.46 ± 0.22	$5.8^{+2.6}_{-1.7}$	6
7	> 550	$1.7^{+1.7}_{-1.0}$	2.2 ± 0.6	0.64 ± 0.36	$0.15^{+0.13}_{-0.1}$	$4.7^{+1.9}_{-1.2}$	6
$N_{\mathrm{b}}\geq 2$, $M_{\mathrm{T}}(\mathrm{b}_{1,2}, E_{\mathrm{T}}^{\mathrm{miss}}) > 175$ GeV, $N_{\mathrm{j}}\geq 5$, $N_{\mathrm{t}}=0$, $N_{\mathrm{W}}\geq 1$							
8	250−450	80 ± 10	28 ± 4	10 ± 5	3.8 ± 32.4	122 ± 35	113
9	> 450	$4.4^{+2.2}_{-1.6}$	5.4 ± 1.4	2.0 ± 1.1	$0.17^{+0.15}_{-0.14}$	12^{+3}_{-2}	15
$N_{\mathrm{b}}\geq 2$, $M_{\mathrm{T}}(\mathrm{b}_{1,2}, E_{\mathrm{T}}^{\mathrm{miss}}) > 175$ GeV, $N_{\mathrm{j}}\geq 5$, $N_{\mathrm{t}}\geq 1$, $N_{\mathrm{W}}=0$							
10	250−450	9.9 ± 3.0	1.1 ± 0.3	1.6 ± 0.8	0.44 ± 2.11	13 ± 4	24
11	> 450	$1.6^{+1.7}_{-0.9}$	0.86 ± 0.32	0.9 ± 0.53	$0.1^{+0.12}_{-0.09}$	$3.5^{+1.8}_{-1.1}$	3
$N_{\mathrm{b}}\geq 2$, $M_{\mathrm{T}}(\mathrm{b}_{1,2}, E_{\mathrm{T}}^{\mathrm{miss}}) > 175$ GeV, $N_{\mathrm{j}}\geq 5$, $N_{\mathrm{t}}\geq 1$, $N_{\mathrm{W}}\geq 1$							
12	> 250	<0.9	$0.37^{+0.22}_{-0.16}$	0.54 ± 0.35	$0.04^{+0.04}_{-0.03}$	$0.95^{+1.07}_{-0.39}$	1

Table 10: Observed events and SM estimates for the aggregate search regions of the low Δm analysis.

Search region	$E_{\mathrm{T}}^{\mathrm{miss}}$ [GeV]	Lost lepton	$\mathrm{Z} \to \nu\nu$	Rare SM	QCD	Total SM	Observed
$N_{\mathrm{b}} \geq 1, N_{\mathrm{b}}^{L} = 1, p_{\mathrm{T}}(\mathrm{ISR}) \geq 250$ GeV, $20 \leq p_{\mathrm{T}}(\mathrm{b}) < 40$ GeV							
0	300−400	96 ± 19	56 ± 8	2.0 ± 1.1	6.4 ± 6.7	161 ± 22	120
1	400−500	17 ± 5	16 ± 3	1.2 ± 0.7	1.8 ± 1.1	36 ± 6	43
2	> 500	10 ± 4	4.8 ± 1.7	0.28 ± 0.23	0.35 ± 0.22	15 ± 5	7
$N_{\mathrm{b}} \geq 1, N_{\mathrm{b}}^{L} = 1, p_{\mathrm{T}}(\mathrm{ISR}) \geq 250$ GeV, $40 \leq p_{\mathrm{T}}(\mathrm{b}) < 70$ GeV							
3	300−400	58 ± 12	21 ± 4	1.4 ± 0.8	3.0 ± 2.6	84 ± 13	75
4	400−500	9.2 ± 3.3	4.5 ± 1.3	0.64 ± 0.41	0.5 ± 0.45	15 ± 4	14
5	> 500	$4.4^{+3.3}_{-2.2}$	1.8 ± 0.5	0.16 ± 0.15	0.14 ± 0.13	$6.5^{+3.3}_{-2.3}$	11
$N_{\mathrm{b}} \geq 1, N_{\mathrm{b}}^{L} \geq 2, p_{\mathrm{T}}(\mathrm{ISR}) \geq 250$ GeV, $40 \leq p_{\mathrm{T}}(\mathrm{b})_1 + p_{\mathrm{T}}(\mathrm{b})_2 < 100$ GeV							
6	300−400	95 ± 17	55 ± 10	4.1 ± 2.1	7.4 ± 5.4	162 ± 21	187
7	400−500	29 ± 7	16 ± 3	1.3 ± 0.7	2.0 ± 1.1	49 ± 8	44
8	> 500	9.8 ± 2.8	7.0 ± 1.6	1.1 ± 0.6	0.43 ± 0.21	18 ± 3	18
$N_{\mathrm{b}} \geq 1, N_{\mathrm{b}}^{L} \geq 2, p_{\mathrm{T}}(\mathrm{ISR}) \geq 250$ GeV, $100 \leq p_{\mathrm{T}}(\mathrm{b})_1 + p_{\mathrm{T}}(\mathrm{b})_2 < 160$ GeV							
9	300−400	115 ± 15	22 ± 4	2.9 ± 1.5	5.8 ± 3.4	146 ± 16	152
10	400−500	27 ± 5	5.6 ± 1.5	1.1 ± 0.6	1.1 ± 0.7	35 ± 5	51
11	> 500	9.6 ± 2.7	1.7 ± 0.6	0.6 ± 0.34	0.25 ± 0.15	12 ± 3	17

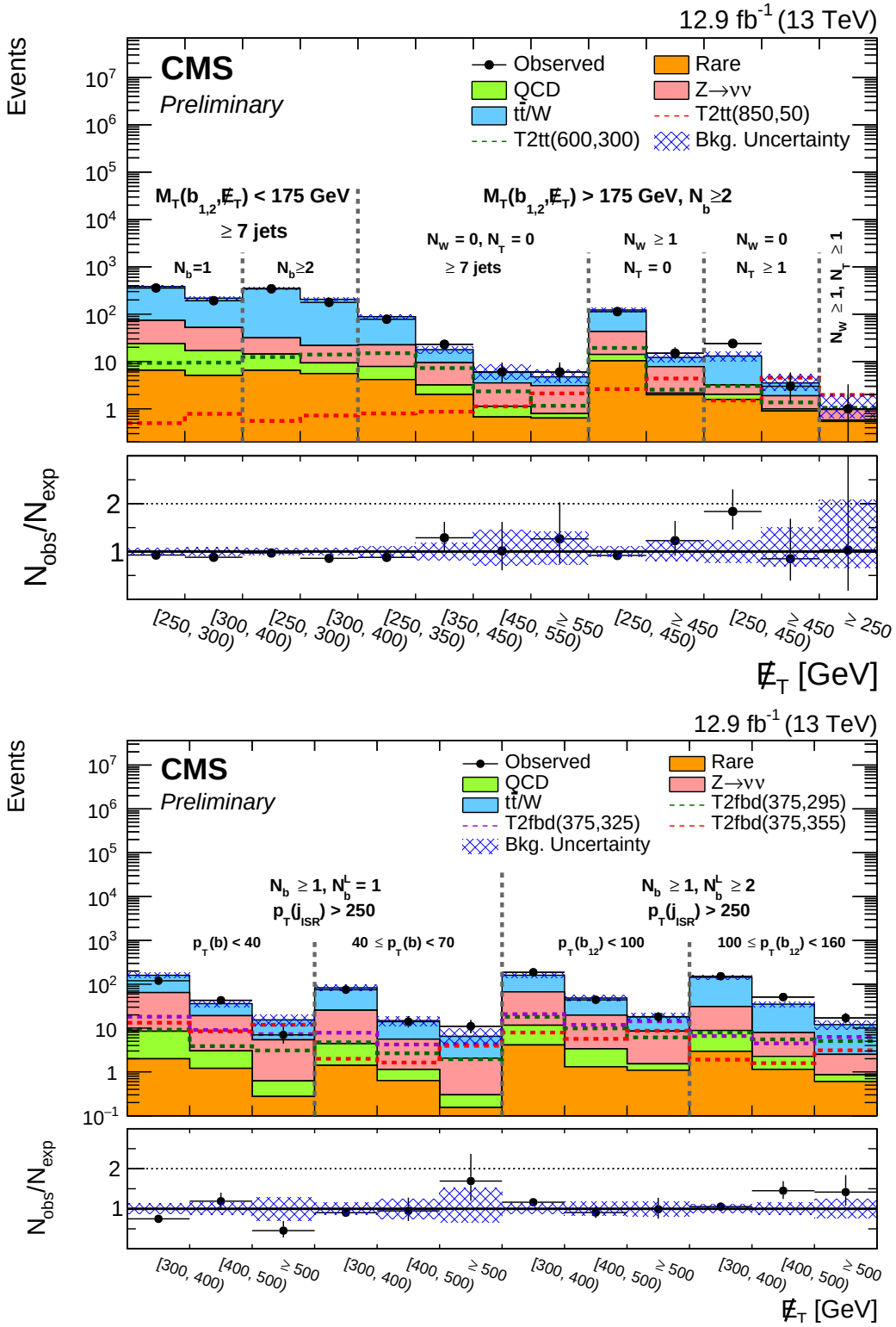

Figure 10: Observed events and SM estimates for the aggregate search regions defined for the high Δm (top) and low Δm (bottom) analyses. The ratios of the observed data to the SM prediction derived from control regions (black points, with error bars corresponding to the data statistical uncertainty) are shown in the ratio plots. The shaded blue band represents the statistical and systematic uncertainty on the background prediction.